# ELECTRIC FIELD INDUCED SPECTRA OF LINEAR AND AXIALLY SYMMETRIC MOLECULES

Thesis for the Degree of Ph. D. MICHIGAN STATE UNIVERSITY PETER LEE WILLSON 1969



## This is to certify that the

#### thesis entitled

Electric Field Induced Spectra
of Linear and Axially Symmetric
Molecules presented by

Peter Lee Willson

has been accepted towards fulfillment of the requirements for

Ph.D. degree in Physics

Major professor

Date July 8, 1969

#### ABSTRACT

# ELECTRIC FIELD INDUCED SPECTRA OF LINEAR AND AXIALLY SYMMETRIC MOLECULES

Ву

#### Peter Lee Willson

Selection rules and line strengths have been calculated for electric field induced spectra (EFS) of axially symmetric and linear molecules. A suitable optical arrangement and appropriate experimental techniques have been developed. Experimental observations of EFS of the linear molecules HCN and DCN and of the axially symmetric molecules CH<sub>3</sub>I, CH<sub>3</sub>Br, CH<sub>3</sub>Cl, CH<sub>3</sub>F, and CH<sub>3</sub>CN were carried out and found to exhibit many of the predicted features.

# ELECTRIC FIELD INDUCED SPECTRA OF LINEAR AND AXIALLY SYMMETRIC MOLECULES

Ву

Peter Lee Willson

## A THESIS

Submitted to
Michigan State University
in partial fulfillment of the requirements
for the degree of

DOCTOR OF PHILOSOPHY

Department of Physics

1969

2 10 156

To My Wife

Ingrid

and Daughter

Susanne

#### ACKNOW LEDGMENT

I wish to express my sincere gratitude to Dr. T.H. Edwards for his guidance, encouragement, and numerous helpful suggestions throughout the course of this research. His constant availability was deeply appreciated. I would also like to thank Drs. P.M. Parker and C.D. Hause for their encouragement and help. The many useful suggestions, especially concerning experimental portions of this work, of my co-workers Richard Peterson, Richard Blank, and Lamar Bullock have also been greatly appreciated. I am very much indebted to the National Aeronautics and Space Administration for the financial support given me in the form of a fellowship.

Finally, I want to express my heart-felt thanks to my wife,
Ingrid, for her patience, understanding, and constant encouragement
and to my parents whose timely help made this all possible.

# TABLE OF CONTENTS

		Page
	LIST OF TABLES	v
	LIST OF FIGURES	vi
Chapte	r	
I	INTRODUCTION	1
11	THEORY OF ELECTRIC FIELD INDUCED SPECTRA	8
III	EXFERIMENTAL TECHNIQUE	44
IV	ELECTRIC FIELD INDUCED SPECTRA OF HCN	56
V	ELECTRIC FIELD INDUCED SPECTRA OF AXIALLY SYMMETRIC MOLECULES	83
VI	CONCLUSIONS	95
	BIBLIOGRAPHY	97

# LIST OF TABLES

Table		Page
(2.1)	Character Table for C <sub>3v</sub> .	21
(2.2)	Direct Product Multiplication Table for C3v.	21
(2.3)	EFS Selection Rules for $c_{3v}$ Symmetry Molecules	25
(2.4)	Line Strengths for $\Delta K = 0$ Electric Field Induced Transitions.	26
(2.5)	Line Strengths for $\Delta K = \pm 1$ Electric Field Induced Transitions.	28
(2.6)	Line Strengths for $\Delta K = \pm 2$ Electric Field Induced Transitions.	31
(2.7)	Line Strengths of EFS Type (c) Transitions	39
(4.1)	EFS Frequencies in $v_3$ and $v_2 + v_3 - v_2$ of HCN.	74
(5.1)	Measured Ratio of $v_4$ and Ground State	
	Electric Dipole Moments for CH <sub>2</sub> F.	94

# LIST OF FIGURES

Figure		Page
(2.1)	Angular Momentum Components of Axially Symmetric Molecules	10
(2.2)	Relationship Between Space-Fixed Coordinates and Molecule-Fixed Coordinates	15
(2.3)	Symmetry of Doubly Excited Degenerate $c_{3v}$	24
(2.4)	Electric Field Induced Line Shapes	41
(3.1)	General EFS Experimental Arrangement	45
(3.2)	Stark Cell	47
(3.3)	Fore-Optical System	52
(4.1)	Normal Vibrational Modes of HCN	57
(4.2)	EFS of $v_3$ and $v_2 + v_3 - v_2$ Bands of HCN	61
(4.3)	Overlapping in P(1) Transition in $v_3$ of HCN	66
(4.4)	Transitions in $\Pi$ - $\Pi$ Band of Linear Molecules	68
(4.5)	Energy Level Diagram of $\Pi$ - $\Pi$ Transitions in a Linear Molecule	71
(4.6)	Transitions in $\Pi$ - $\Sigma$ Band of Linear Molecule	76
(4.7)	EFS of $v_2 + v_3$ and $2v_2 + v_3 - v_2$ Bands of HCN	79
(4.8)	Overlapping in EFS R(0) Transition in $v_2 + v_3$ Band of HCN	80
(4.9)	Tracing of Low Pressure HCN $v_2 + v_3$ Band Induced Q Branch	80
(5.1)	EFS of $v_1$ and $v_4$ Bands of $CH_3I$	86
(5.2)	ν, and ν, Absorption Bands of CH,I	87

#### CHAPTER I

#### INTRODUCTION

This thesis is concerned with the theory and experimental observation of electric field induced spectra (EFS) of linear and axially symmetric molecules in the near infrared region.

Qualitative features of the theory and method of experimental observation are outlined in this chapter. A short description of the Stark effect is included because of its influence on electric field induced line shapes and line strengths, and finally the Kerr effect is discussed for the sake of completness.

Chapter II contains a detailed development of the theory of electric field induced spectra for axially symmetric molecules with linear molecules included as a special case.

The remainder of this work is devoted to a description of the experiments performed and the interpretation of EFS obtained for the linear molecules HCN and DCN and for the axially symmetric molecules  $\operatorname{CH}_3F$ ,  $\operatorname{CH}_3Br$ , and  $\operatorname{CH}_3I$ .

#### ELECTRIC FIELD INDUCED SPECTRA

In 1932 E.U. Condon (1) proposed production of infrared molecular spectra by application of an electric field. He pointed out that the resulting spectra should exhibit selection rules differing from those of field-free absorption spectra.

Infrared vibrational absorption spectra arise from changes in the electric dipole moment due to excitation of one or more

quanta of vibrational energy. The probability of a radiative transition occurring between two vibrational states is proportional to the square of the matrix element of the electric dipole moment between the two vibrational states. If the molecule is placed in an electric field, another contribution to the electric dipole moment is induced which is related linearly to the vector components of the applied field through the molecular polarizability tensor. The probability that a different radiative transition may occur while the molecule is in an electric field is proportional to the square of the matrix element of the induced dipole moment. Because of the linear relationship between the induced dipole moment and the field, the intensities of the new radiative transitions are proportional to the square of the magnitude of the electric field.

Inducing an electric dipole moment in a molecule has three important consequences. First, if a molecule has no dipole moment in any vibrational state (such as the homopolar diatomic molecules  $H_2$ ,  $D_2$ ,  $O_2$ , etc.), an otherwise unattainable infrared absorption spectrum may be induced. Crawford and Mac Donald (2) and Terhune and Peters (3) produced infrared  $H_2$  spectra by this method. Secondly, molecules either possessing a permanent dipole moment or having a dipole moment in particular states due to vibration (such as  $CO_2$ ) have possible radiative transitions that are not otherwise allowed because in this case selection rules are determined by matrix elements of the polarizability tensor instead of by the dipole moment vector. Finally, the intensities of even those transitions allowed in the absence of the field are modified by the presence of the field.

The usual technique of detecting non-induced absorption spectra is to interrupt the absorption signal periodically with a mechanical light chopper to provide a pulsed signal for phase sensitive detection and amplification. On the other hand, for EFS, the absorption coefficient is proportional to the square of the applied electric field, an ac electric field produces an "internal" modulation at twice the applied field frequency. Omission of the mechanical light chopper and application of an ac electric field, therefore, produces a signal at the detector made up of a large dc component corresponding to field-free absorption and a small ac component at twice the field frequency corresponding to induced intensity changes. Phase sensitive ac detection and amplification of this "modulated dc" signal eliminates the large dc component and leaves only that part of the absorption signal arising from the field. The ac signal is the difference between the signal due to absorption with the field on and the signal due to absorption with the field off. This "difference spectrum" technique of detection of electric field induced spectra was used in the experimental portion of this work.

#### STARK EFFECT

The Stark effect describes the changes in rotational energy of a molecule due to the interaction of the molecular dipole moment with the applied field. The interaction Hamiltonian is given by:

$$H_{int} = -\mu F \cos \theta \qquad (1.1)$$

where  $\mu$  is the electric dipole moment, F is the magnitude of the electric field, and  $\theta$  is the angle between F and  $\mu$ . In

the absence of an external field, the molecular electric dipole moments have random spatial orientations and the rotational energy levels have an essential degeneracy. The application of an electric field defines a spatial direction along which the dipole moments tend to align through interaction with the field thereby lifting the rotational degeneracy. Therefore, a transition between two previously degenerate rotational energy levels would exhibit fine structure in the presence of an electric field if sufficient resolving power were available.

If the wave functions for a molecule in the presence of an electric field were known explicitly, the change in energy of any rotational state could be calculated exactly. Unfortunately, this is never the case and approximate methods similar to those described below must be employed.

The most common treatment of Stark energy shifts for polar axially symmetric molecules is the weak field approximation. In this approximation, the interaction Hamiltonian is assumed to be small in comparison to the separation of rotational energy levels and quantum mechanical perturbation theory is invoked, c.f. (4). To second order in the field, the change in energy is given by perturbation theory as:

$$\Delta E = -\frac{\mu FMK}{J(J+1)} + \frac{\mu^2 F^2}{2hcB} \left\{ \frac{(J^2 - K^2)(J^2 - M^2)}{J^3(2J - 1)(2J + 1)} - \frac{[(J+1)^2 - K^2][(J+1)^2 - M^2]}{(J+1)^3(2J+1)(2J+3)} \right\}$$
(1.2)

where  $\mu$  is the permanent electric dipole moment. F is the magnitude of the electric field, B is the inverse of the principal

moment of inertia about an axis perpendicular to the molecular symmetry axis in units of cm<sup>-1</sup>, h is Planck's constant, and J, K, and M are the rotational quantum numbers (J is the total rotational angular momentum quantum number, K is the projection of J along the molecular symmetry axis, and M is the "magnetic" quantum number - the projection of J along the direction defined by the electric field). For a linear molecule possessing a permanent electric dipole moment, K = 0, and no first order Stark effect is possible. The above formula (1.2) for a linear molecule simplifies to

$$\Delta E = \frac{u^2 F^2}{2hcBJ(J+1)} \left\{ \frac{J(J+1) - 3M^2}{(2J-1)(2J+3)} \right\}$$
 (1.3)

An exact solution of the Stark effect problem is available, but is not in closed form. This method is attributed to W.E. Lamb and a detailed discussion is given by Maker (5). The energy expression is in the form of an infinite continued fraction.

Shirley (6) has numerically evaluated this expression for the few rotational states through J = 4.

#### KERR EFFECT

The Kerr effect refers to the optical birefrigence exhibited by gases, liquids, and solids in the presence of an electric field (electro-optical birefrigence). The observable in Kerr effect experiments is the phase difference between electric vector components parallel and perpendicular to the electric field,  $F_Z$ , of a light beam initially plane polarized at an angle of  $45^{\circ}$  with respect to  $F_Z$  after passing through a medium of length L.

The theoretical details of this effect are given by Buckingham (7) and Dows and Buckingham (8). The following discussion is taken from those papers.

The difference in phase  $\delta$  of the electric vector components parallel and perpendicular to the field direction of initially plane polarized light after passage through the gas sample is given by:

$$\delta = 2\pi L(n_Z - n_X)/\lambda = 2\pi LBF_Z^2$$
 (1.4)

where L is the path length,  $\lambda$  is the wave length of the radiation in vacuo,  $(n_Z - n_X)$  is the difference between refractive indices of the medium parallel and perpendicular to the field, respectively, and B is the Kerr "constant". The Kerr constant exhibits considerable dispersion.

For frequencies of incident radiation far removed from those of strong absorption bands of non-isotropic polar molecules, the dominating process in the dispersion of the Kerr constant B is the tendency for the molecular dipole moments to align along the field direction. Dispersion of the Kerr constant in this case is strongly temperature dependent  $(I^{-2})$  and its measurement leads to a knowledge of the anisotropy,  $(\alpha_{\parallel} - \alpha_{\perp})$ , of the polarizability tensor  $\alpha_{ij}$ .

The Kerr constant for frequencies of incident radiation near those of strong absorption bands, on the other hand, is temperature independent and the dominating contribution to dispersion of the "constant" B is due to distortion of the molecule by the electric field. Quantitative measurements of the dispersion in this instance would provide values of excited state electric dipole moments. Qualitative observation of the dispersion in this

region would provide information on the direction of the transition dipole moment with respect to the molecular axes as the increase or decrease of the Kerr constant with increasing frequency in the vicinity of an absorption line is governed by the direction of the transition moment.

The phase difference  $\delta$  is proportional to the square of the magnitude of the applied electric field (1.4) and the same ac experimental detection techniques could be used for Kerr effect experiments as are used for electric field induced spectra. Some method of taking into account the polarizing effects of a long narrow Stark cell would be necessary for successful Kerr effect data interpretation.

#### CHAPTER II

#### THEORY OF ELECTRIC FIELD INDUCED SPECIRA

The theory of electric field induced spectra will now be considered in detail. The line strengths of transitions not allowed in the absence of an external field and the corrections to the line strengths of transitions allowed in the absence of the field will be calculated for axially symmetric molecules and particularized for linear molecules as needed. The calculated line strengths are given in Tables 2.4 through 2.6. Selection rules obeyed by the rotational quantum numbers will be derived qualitatively and then rigorously. Finally, expected line shapes will be described.

#### LINE STRENGTHS

As a starting point, the integrated absorption coefficient  $k(\nu) \quad \text{of an absorption line will be needed.} \quad \text{For a transition from}$  state m to state  $m^2$ , this coefficient is

$$k(v)_{m}^{m^{1}} = \left(\frac{N_{m}}{2J+1}\right) h_{v_{mm}} B_{m}^{m^{1}}$$
 (2.1)

where  $N_m$  is the population of the m-1 state,  $v_{mm}$  is the frequency of the absorption line, and h is Planck's constant.  $B_m^{m^2}$  is the Einstein coefficient of induced absorption, which can be calculated using time-dependent perturbation theory. For absorption of radiation polarized in the space-fixed  $\xi$  direction (X,Y, or Z) by a gas of axially symmetric molecules, the Einstein B coefficient is given by

$$B_{\tau,v,R}^{\tau',v',R'} = \frac{8\pi^3}{h^2} | \langle \tau, v, R | \mu_{\xi} | \tau', v', R' \rangle |^2 , \qquad (2.2)$$

where the unprimed quantities refer to the lower state and the primed quantities refer to the upper state. The electronic and vibrational quantum numbers are symbolized, respectively, by  $\tau$  and v. R is used to abbreviate the rotational quantum numbers J, K, and M; where J is the total rotational angular momentum quantum number, K is the quantum number of projection of the total angular momentum along the molecular symmetry axis, and M is the quantum number of the projection of the angular momentum along the spatial axis defined by the electric field.  $\mu_{\xi}$  is the electric dipole moment operator along the space-fixed  $\xi$  (X,Y,Z) direction and  $<\tau$ ,v,R $|\mu_{\xi}|\tau'$ ,v',R'> is the transition moment for radiation polarized in the space-fixed  $\xi$  direction. The angular momenta are shown graphically in Figure (2.1).

The problem of calculating intensities of transitions allowed in the presence of an external electric field is therefore one of evaluating the line strengths  $|<\tau,v,R|\mu_{\xi}|\tau',v',R'>|^2$  in a suitably chosen basis set of perturbed eigenfunctions.

Using rigid rotator harmonic oscillator wave functions as the zero-order basis and  $-\mu_Z^F_Z$  as the perturbation, the perturbed eigenfunctions (to second order in the magnitude  $F_Z$  of the electric field applied along the space-fixed Z-direction) have the form

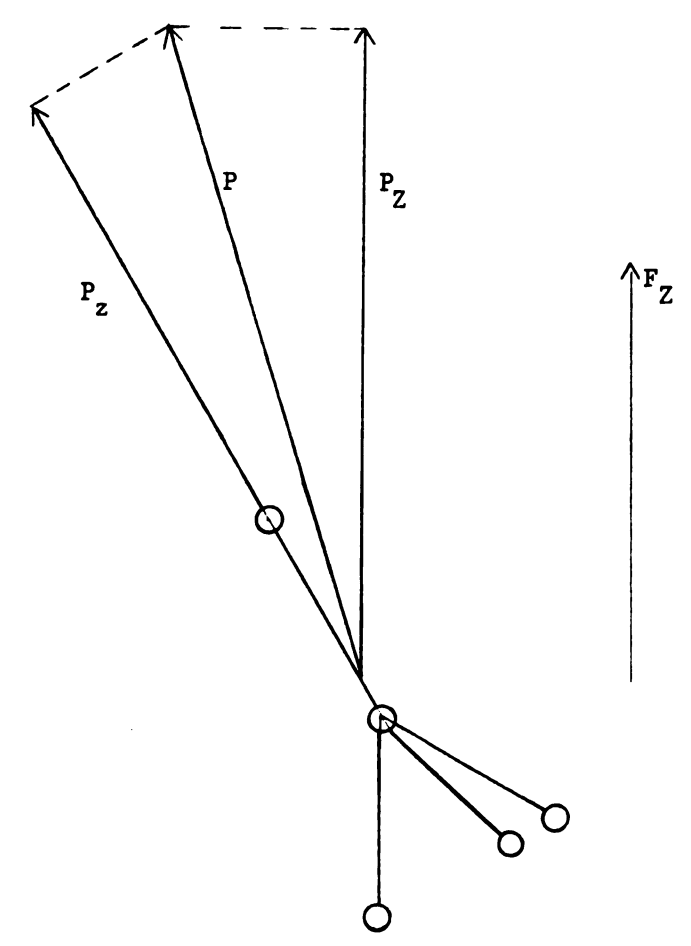


Figure 2.1 Angular Momentum Components of Axially Symmetric Molecules.

 $P = \sqrt{J(J+1)} \frac{h}{2\pi}$  total angular momentum.

projection of P on molecular symmetry axis.

 $P_{z} = K \frac{h}{2\pi}$   $P_{z} = M \frac{h}{2\pi}$ projection of  $\, P \,$  along field defined spatial  $\, Z \,$  axis.

$$\begin{split} \Psi_{\tau,v,R}(F_{Z}) &= \Psi_{\tau,v,R} + F_{Z} \sum_{\tau'',v'',R''} \frac{\langle \tau'',v'',R'' | \mu_{Z} | \tau,v,R \rangle}{\ln c v_{\tau,v,R}^{\tau'',v'',R''}} \Psi_{\tau'',v'',R''} \\ &+ F_{Z}^{2} \sum_{\tau'',v'',R''} \sum_{\tau''',v''',R''} \frac{\langle \tau''',v'',R'' | \mu_{Z} | \tau'',v'',R'' | \nu_{Z} | \tau'',v'',R'' | \nu_{Z} | \tau,v,R \rangle}{\ln^{2} c^{2} v_{\tau,v,R}^{\tau''',v''',R'''} v_{\tau,v,R}^{\tau''',v''',R'''}} \end{split}$$

$$-\frac{1}{2} F_{Z}^{2} \sum_{\tau'',v'',R''}^{\prime} \frac{\left| \langle \tau'',v'',R'' | \mu_{Z} | \tau,v,R \rangle \right|^{2}}{h^{2} c^{2} (v_{\tau,v,R}^{\prime\prime\prime})^{2}} \cdot \Psi_{\tau,v,R}$$
 (2.3)

where the prime on the summation indicates exclusion of the state  $\tau, v, R$ .

Using the perturbed wave functions (2.3), the transition moment has the form:

$$<\tau, v, R|\mu_{g}|\tau', v', R'> = <\tau, v, R|\mu_{g}|\tau', v', R'>_{o} + <\tau, v, R|\mu_{g}|\tau', v', R'>_{F_{7}}$$
 (2.4)

where  $<\tau,v,R|\mu_g|\tau',v',R'>_o$  is the transition moment of transitions allowed in the absence of the field (unperturbed transition moment) and  $<\tau,v,R|\mu_g|\tau',v',R'>_F$  includes the correction to the transition moment due to the field for transitions allowed in the absence of the field, as well as the transition moment of transitions not allowed in the absence of the field.

This work is concerned with the second term of (2.4) which is given by:

$$\langle \tau, v, R | \mu_{g} | \tau', v', R' \rangle_{F_{Z}} = 
F_{Z} \sum_{\tau'', v'', R''}^{\prime} \frac{\langle \tau, v, R | \mu_{Z} | \tau'', v'', R'' \times \tau'', v'', R'' | \mu_{g} | \tau', v', R' \rangle}{\text{hc}_{v}_{\tau, v, R}^{\tau'', v'', R''}}$$

$$+ F_{Z} \sum_{\tau'', v'', R''}^{\prime} \frac{\langle \tau, v, R | \mu_{Z} | \tau'', v'', R'' \times \tau'', v'', R'' | \mu_{Z} | \tau', v', R' \rangle}{\text{hc}_{v}_{\tau'', v'', R''}^{\tau'', v'', R''}}$$
(2.5)

to lowest order in  $F_Z$ . The doubly primed quantities refer to the intermediate states through which the unprimed (lower) and primed (upper) states are coupled by the perturbation,  $-\mu_2F_2$ .

Dows and Buckingham (9) have shown that the terms in the sums of equation (2.5) can be separated into three types, viz.,

$$\langle \tau, v, R | \mu_{g} | \tau', v', R' \rangle = \gamma_{g} + \delta_{g} + \lambda_{g}$$
 (2.6)

with the following conditions imposed on the terms:

Part 
$$\gamma_g$$
:  $\tau'', v'' = \tau, v$  in first sum of (2.5)
$$\tau'', v'' = \tau', v'$$
 in second sum of (2.5)

Part  $\delta_g$ :  $\tau'' = \tau$  in first sum of (2.5)
$$\tau'' = \tau'$$
 in second sum of (2.5)

Part  $\lambda_g$ :  $\tau'' \neq \tau$  in first sum of (2.5)
$$\tau'' \neq \tau'$$
 in second sum of (2.5).

Part  $\gamma_{\xi}$  results from the mixing of rotational wavefunctions within the same vibronic state (vibrational and electronic quantum numbers are unchanged) through the perturbation; part  $\delta_{\xi}$  arises from the mixing of rotational wavefunctions belonging to different vibrational states but within the same electronic state; and part  $\lambda_{\xi}$  results from the mixing of rotational wavefunctions belonging to different

electronic states through the perturbation. Because of the relative magnitudes of the energy denominators,  $\gamma_{\xi} \gg \delta_{\xi} \gg \lambda_{\xi}$  in all cases where the Born-Oppenheimer approximation is valid. For polar molecules, therefore,  $\gamma_{\xi}$  will predominate, whereas for non-polar molecules,  $\lambda_{\xi}$  is the only non-zero term. The explicit forms of  $\gamma_{\xi}$ ,  $\delta_{\xi}$ , and  $\lambda_{\xi}$  were given by Dows and Buckingham (9).

$$\gamma_{g} = F_{Z} \left\{ \sum_{R'' \neq R}^{1} \frac{\langle \tau, v, R | \mu_{Z} | \tau, v, R'' | \omega_{T}, v, R'' | \mu_{g} | \tau', v', R' \rangle}{hcv_{R}^{R''}} + \sum_{R'' \neq R'}^{1} \frac{\langle \tau, v, R | \mu_{g} | \tau', v', R'' | \omega_{T}', v', R'' | \mu_{Z} | \tau', v', R' \rangle}{hcv_{R'}^{R''}} \right\}, (2.7)$$

$$\delta_{g} = F_{Z} \left\{ \sum_{v'' \neq v}^{1} \frac{\langle \tau, v, R | \mu_{Z} | \tau, v'', R'' | \omega_{T}, v'', R'' | \mu_{g} | \tau', v', R' \rangle}{hcv_{v, R}^{V'', R''}} + \sum_{v'' \neq v'}^{1} \frac{\langle \tau, v, R | \mu_{g} | \tau', v'', R'' | \omega_{T}', v'', R'' | \mu_{Z} | \tau', v' | R' \rangle}{hcv_{v, R}^{V'', R''}} \right\} (2.8)$$

$$\lambda_{g} = F_{Z} \left\{ \sum_{\tau'' \neq \tau}^{1} \sum_{v'', R} \frac{\langle \tau, v, R | \mu_{Z} | \tau'', v'', R'' | \omega_{T}'', v'', R'' | \mu_{g} | \tau', v', R' \rangle}{hcv_{\tau, v}^{T'', v'', R''}} + \sum_{\tau'' \neq \tau}^{1} \sum_{v'', R} \frac{\langle \tau, v, R | \mu_{g} | \tau'', v'', R'' | \omega_{T}'', v'',$$

From these expressions (2.7), (2.8), and (2.9) the selection rules obeyed by the rotational quantum numbers for transitions in the presence of an external electric field may be deduced.  $\lambda_{\bf g}$  is an expression for the matrix elements of the polarizability tensor of an axially symmetric molecule (10). Therefore, in the case of a non-polar molecule where  $\lambda_{\bf g}$  is the only surviving term, the selection rules obeyed by the rotational quantum numbers in electric field

induced spectra are the same as those of Raman scattering. In this case, electric field induced spectra can be thought of as Raman spectra in the limit where the frequency of incident radiation approaches zero, as E.U. Condon (1) pointed out. Since  $\gamma_g$  and  $\delta_g$  are the same functions of the rotational matrix elements as  $\lambda_g$ ; electric field induced spectra obey the selection rules of the Raman effect in general, but the intensities are different due to the energy difference denominators in  $\gamma_g$  and  $\delta_g$ .  $\lambda_g$  is the transition moment for the Raman effect and the line strengths for this effect have been given by Placzek and Teller (11).

In all cases, evaluation of the matrix elements may be accomplished by expressing the dipole moment operators in terms of molecular-fixed coordinates:

$$\mu_{\mathbf{A}} = \sum_{\alpha = \mathbf{X}, \mathbf{Y}, \mathbf{Z}} \mathbf{a}_{\mathbf{A}\alpha} \mu_{\alpha} \tag{2.10}$$

where A = X,Y,Z (space-fixed coordinates), and the  $a_{AQ}$  are the direction cosines between the molecule-fixed coordinates (lower case subscript) and space-fixed coordinates, whose matrix elements are well known (cf. Strandberg (12) or Townes and Schawlow (4)). The relationship between the two coordinate systems is shown in Figure (2.2).

#### POLAR MOLECULES

When the relevant transition moment  $\gamma_{\xi}$  for molecules having a permanent dipole moment (which must lie along the (z) symmetry axis) is written in terms of molecule-fixed coordinates, each summation in equation (2.7) becomes a summation over nine terms.

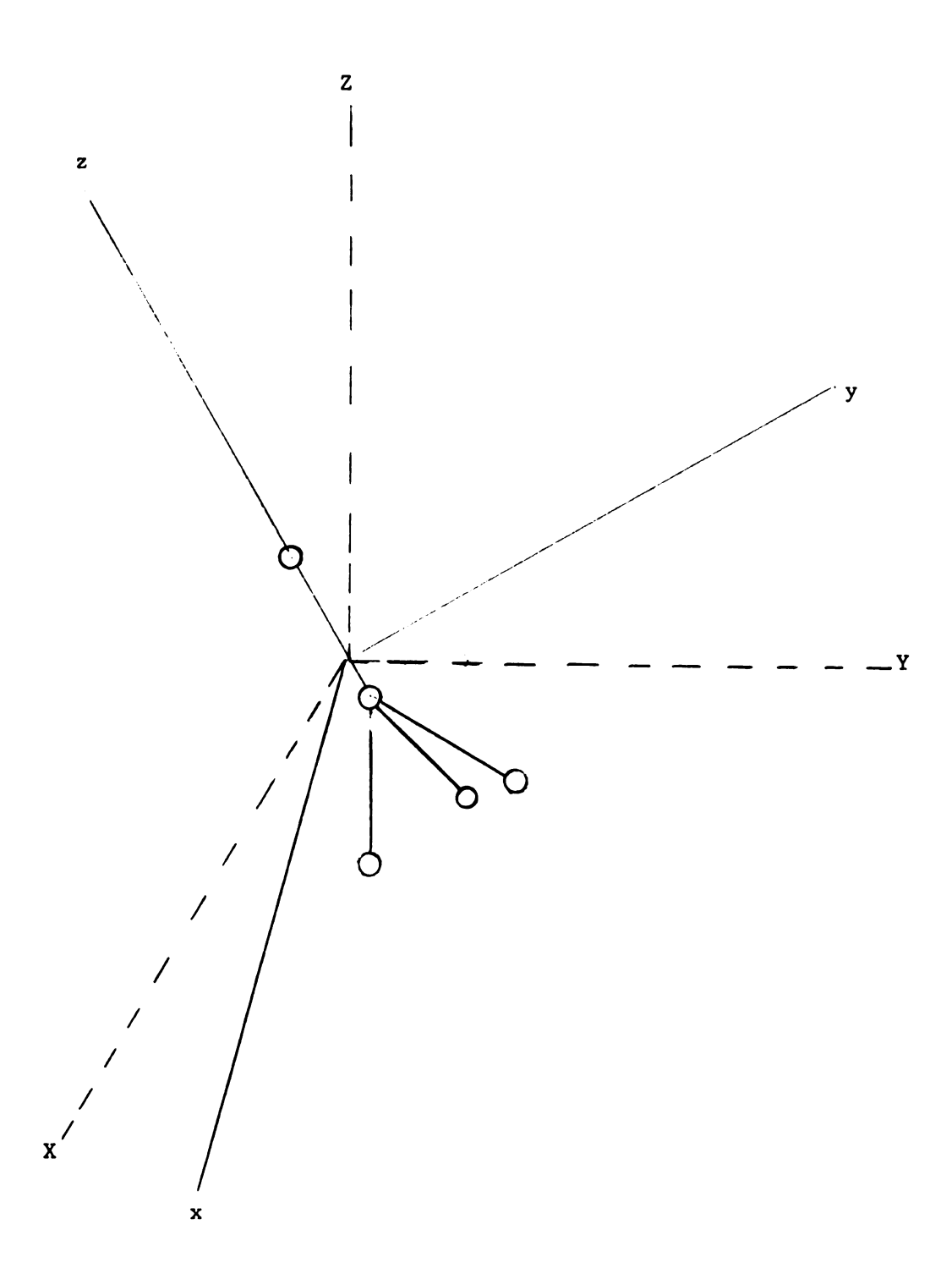


Figure 2.2. Relationship between space-fixed coordinates X,Y, and Z and molecule-fixed coordinates x,y, and z.

A convenient separation of  $\gamma_{\xi}$  into two terms characteristic of the type of transition involved is possible.

$$\gamma_{\xi} = \|\gamma_{\xi} + \bot \gamma_{\xi}; \qquad (2.11)$$

includes all terms containing  $\mu_z$  and  $\mu_z^!$ , and  $\mu_z^!$  includes all terms containing  $\mu_x = \mu_y$  and  $\mu_x^! = \mu_y^!$ , where the  $\mu_\alpha$  and  $\mu_\alpha^!$  are dipole moment expectation values, viz.,

$$\mu_{\alpha} = \langle \tau, v | \mu_{\alpha} | \tau, v \rangle$$
 and  $\mu_{\alpha}' = \langle \tau', v' | \mu_{\alpha} | \tau', v' \rangle$ .

Finally, the  $\|\gamma_{\xi}\|$  and  $\|\gamma_{\xi}\|$  can then be further separated according to the selection rules on K, which may be determined by inspection of the direction cosine matrix elements, so that

$$\| Y_{\xi} = (\| Y_{\xi})^{K'=K} + (\| Y_{\xi})^{K'=K+1}$$
 (2.12)

$$_{\perp Y_{\xi}} = (_{\perp Y_{\xi}})^{K'=K} + (_{\perp Y_{\xi}})^{K'=K+1} + (_{\perp Y_{\xi}})^{K'=K+2}$$
 (2.13)

where

$$(||\gamma_{\xi})^{K'=K} = F_{Z} < \tau . \forall |\mu_{z}| \tau', \forall ' > \left\{ \mu_{z} \sum_{R'' \neq R}^{t} \frac{\langle R | a_{Zz} | R'' \times R'' | a_{\xi z} | R' \rangle}{hcv_{R}^{R''}} + \mu_{z}^{t} \sum_{R'' \neq R'}^{t} \frac{\langle R | a_{\xi z} | R'' \times R'' | a_{\zeta z} | R' \rangle}{hcv_{R'}^{R''}} \right\}$$

$$(2.14)$$

$$F_{Z} < \tau, v | \mu_{X} | \tau', v' > \left\{ \mu_{Z} \sum_{R'' \neq R}^{\prime} \frac{\langle R | a_{ZZ} | R'' > R'' | (a_{gx} + a_{gy}) | R' >}{hcv_{R}^{R''}} + \mu_{Z}^{\prime} \sum_{R'' \neq R'}^{\prime} \frac{\langle R'' | a_{ZZ} | R' > R | (a_{gx} + a_{gy}) | R'' >}{hcv_{R}^{R''}} \right\}$$

$$+ \mu_{Z}^{\prime} \sum_{R'' \neq R'}^{\prime} \frac{\langle R'' | a_{ZZ} | R' > R | (a_{gx} + a_{gy}) | R'' >}{hcv_{R}^{R''}}$$
(2.15)

and

The selection rules on J, the total angular momentum, in equations (2.14) through (2.17) may be seen by inspection of the direction cosine matrix elements to be  $\Delta J = 0$ ,  $\pm 1$ ,  $\pm 2$  (with the obvious restriction that J and J' must remain non-negative and  $K \leq J$ ) as in the Raman effect. The conditions under which the various  $\Delta K$  transitions can take place and the line strengths appropriate to these conditions are obtained using symmetry considerations in the section which follows.

If individual Stark effect transitions (transitions between lower and upper state M values) are resolvable, the electric field induced line strengths for the various transitions possible in polar axially symmetric molecules are given by individual terms such as

(|| or 
$$\Gamma_g$$
)  $\Gamma_{J,K,M,T,V}^{J',K',M',T',V'} = | (|| or  $\Gamma_{Y_g}$ )  $\Gamma_{K}^{K'}$  | 2. (2.18)$ 

In the near infra-red region, however, Stark effect frequency shifts are seldom as large as the line width due to pressure broadening (13), especially under our experimental conditions where the Stark cell was pressurized to 1/2 atm. with  ${\rm SF}_6$  to prevent electrical breakdown. Thus, to a very high degree of approximation, a molecular absorption line in the presence of an external electric field can be characterized by a line strength, a central frequency, and a line shape whose origin and form are related to the amount of Stark broadening it suffers. The effect of Stark splitting on line shape is discussed later. Under the assumption of small Stark splitting, the M degeneracy can be treated as remaining and equation (2.18) must be summed over M and M'; the lower and upper state degeneracies, respectively. Listed for  ${\rm C}_{3{\rm V}}$  symmetry molecules in tables (2.4 through 2.6) are my calculated values of the allowed

$$(\| \text{ or } _{\perp}\Gamma_{\xi})_{J,K,\tau,v}^{J^{?},K^{?},\tau',v'} = \| (\| \text{ or } _{\perp}\gamma_{\xi})^{K^{?}} \|^{2};$$
 (2.19)

the line strengths of transitions not allowed in the absence of an external electric field to lowest order in the field and the lowest order correction to the line strengths of transitions allowed in the absence of the field. The tables may be used for electronic transitions in their given form. For rotation-vibration spectra  $\tau' = \tau$  and for pure rotation spectra  $\tau' = \tau$  and v' = v.

A partial check of the results for the  $(\|\Gamma_{\xi})$  was obtained by comparison with the results of Dows and Buckingham (9) for diatomic molecules by setting K=0 in the tabulated expressions. In addition, the quantum dependence of the  $(\|\Gamma_{\xi})$  and  $({}_{1}\Gamma_{\xi})$ , for the most part, could be checked with the Raman line strengths given by

Placzek and Teller (11) because in the Raman effect, as in electric field spectra, a sum over M and M' of the product of two direction cosine matrix elements occurs. The energy difference denominators in the electric field induced intensities prevent comparison with the  $\Delta J = 0$  Raman values. Complete agreement in quantum dependence was found in all cases which could be compared.

#### SELECTION RULES

The discussion of electric field induced spectra will now be restricted to fundamental and overtone vibration-rotation bands  $(\tau = \tau^*)$  in molecules possessing  $C_{3v}$  symmetry; specifically, those molecules having the form XYZ<sub>3</sub>. The following discussion uses elementary group theoretical arguments to predict the selection rules tabulated in Table (2.3).

The line strengths,  $(\Gamma_Z)$ , are proportional to the square of the product of a diagonal matrix element,  $<\tau v | M_{\beta_i} | \tau v>$ , and an off diagonal matrix element,  $<\tau v | M_{\beta_j} | \tau v'>$ . A useful theorem from group theory can be applied to these matrix elements to determine the conditions under which they must vanish. These conditions yield the required set of selection rules. The theorem states that if  $\Psi_{n\alpha_i}$ ,  $\Psi_{n'\alpha'i}$ , and  $\Psi_{\beta_j}$  are partners in bases for the irreducible representations of a group, then  $<\Psi_{n\alpha_i}|_{M_{\beta_j}}|_{\Psi_{n'\alpha'i'}}>=0$  provided the direct product representation  $\Gamma_{\alpha}^* \times \Gamma_{\beta} \times \Gamma_{\alpha'}$ , does not contain  $\Gamma_1$ , the trivial representation (14). In a simpler form this rule states that the direct product representation  $\Gamma_{\alpha}^* \times \Gamma_{\alpha'}$ , must transform, or have component that transforms, like  $\Gamma_{\beta}$ , for the matrix element to be non-zero (15).

Application of the above theorem requires knowledge of the transformation properties of the three components of the dipole moment operator, the transformation properties of the normal vibrations, and the direct product multiplication table of the irreducible representations of the group under consideration.

Table (2.1) is the character table for the  $C_{3\nu}$  point group.

From the definition of the components of the dipole moment operator;

$$\mu_x = \sum_i e_i x_i,$$
 $\mu_y = \sum_i e_i y_i,$ 
 $\mu_z = \sum_i e_i z_i;$ 

where  $e_i$  is the charge of the particle having coordinates  $x_i, y_i$ , and  $z_i$  and the character table for  $C_{3v}$ , it is clear that  $\mu_x, \mu_y$ , and  $\mu_z$  have the same behavior with respect to symmetry operations as the translations  $T_x$ ,  $T_y$ , and  $T_z$ , respectively. Therefore,  $\mu_x$  and  $\mu_y$  transform according to E, the doubly degenerate irreducible representation of  $C_{3v}$ , and  $\mu_z$  transforms according to  $A_1$ , the totally symmetric irreducible representation of  $C_{3v}$  (16).

The degenerate normal vibrational modes of molecules possessing  $C_{3v}$  symmetry must transform according to E, the only two dimensional irreducible representation of  $C_{3v}$ . There are two choices according to which the non-degenerate vibrations could transform -  $A_1$  and  $A_2$ . Since  $A_2$  is the irreducible representation of rotations about the symmetry axis,  $R_z$ , the only true  $A_2$  type vibrations are torsional modes. Therefore, molecules of the form XYZ<sub>3</sub> will have no true vibrational modes that transform according to  $A_2$  and all non-degenerate vibrational modes must transform according to  $A_1$  (16).

c <sub>3v</sub>			E	<sup>2C</sup> 3	3σ <sub>v</sub>
$x^2 + y^2, z^2$	Z	A <sub>1</sub>	1	1	1
	Rz	A <sub>2</sub>	1	1	-1
$x^2 - y^2$ , xy xz, yz	х,у Rx, Ry	E	2	-1	0

TABLE 2.1 Character Table for  $c_{3v}$ 

	A <sub>1</sub>	A <sub>2</sub>	E
A <sub>1</sub>	A <sub>1</sub>	A <sub>2</sub>	E
A <sub>2</sub>	A <sub>2</sub>	A 1	E
E	E	E	$A_1 + A_2 + E$

TABLE 2.2 Direct Product Multiplication Table for  $C_{3v}$ 

The direct product multiplication table for  $C_{3v}$  can be determined using the character table, Table (2.1), and is shown in Table (2.2).

Application of the above theorem to the diagonal matrix elements  $\mu_{\alpha} = \langle \text{Tv} | \mu_{\alpha} | \text{Tv} \rangle$  and  $\mu_{\alpha}' = \langle \text{Tv}' | \mu_{\alpha} | \text{Tv}' \rangle$ , shows that  $\mu_{Z}$  and  $\mu_{Z}'$  are never necessarily zero, whereas,  $\mu_{X}$  is always zero and  $\mu_{X}'$  can only be non-zero if v' refers to an upper vibrational state that transforms, or has a component that transforms, according to E. Simple physical arguments yield the same result. The average value of the dipole moment vector in the ground state is the component along the molecular symmetry axis.  $\mu_{X}'$ , on the other hand, can only be non-zero in upper vibrational states that induce a dipole moment perpendicular to the molecular symmetry axis.

In non-degenerate fundamental and overtone vibrational modes, both v and v' transform according to  $A_1$ ; therefore, only the diagonal and off diagonal matrix elements of  $\mu_z$  are non-zero. Examination of equations (2.14) through (2.17) shows that only (2.14) satisfies this criterion and hence  $\Delta K = 0$  transitions are the only possibility in non-degenerate fundamental and overtone bands.

Singly and multiply excited degenerate vibrations have an associated vibrational angular momentum  $\ell$  that must be considered in conjunction with other symmetry considerations in any selection rule calculation. For the degenerate vibration  $v_i$ , the associated vibrational angular momentum  $\ell_i$  can take on values

$$L_i = \pm v_i + \pm (v_i - 2), \pm (v_i - 4), \dots 0 \text{ or } \pm 1;$$

where  $v_i$  is the number of vibrational quanta of the  $v_i$  mode excited (Herzberg p. 81, 16). Amat's rule relating  $\Delta K$  and  $\Delta C$  for  $C_{3v}$  symmetry is given by (17)

$$\Delta K - \sum_{i} M_{i} = \pm 3p$$

where p is an integer and  $M_i = \ell_i$  because  $\ell$  of the rovibronic ground state is zero.

In a degenerate fundamental vibration, as previously mentioned,  $\mu_{x}^{-1}$ ;  $\mu_{z}^{-1}$ ; and  $\mu_{z}^{-1}$  are non-zero and  $\ell$  has values  $\ell=\pm 1$ . Consideration of the transformation properties of the matrix element  $\langle \tau, v | \mu_{\alpha} | \tau, v^{-1} \rangle$  shows that  $\langle \tau, v | \mu_{z} | \tau, v^{-1} \rangle = 0$ , whereas,  $\langle \tau, v | \mu_{x} | \tau, v^{-1} \rangle$  is not necessarily zero because v transforms according to  $A_{1}$  and  $v^{-1}$  transforms according to E. Examination of equations (2.14) through (2.17) shows that (2.15),  $\Delta K = \pm 1$ , and (2.16).  $\Delta K = 0$ ,  $\pm 2$ , both satisfy the above conditions. Application of Amat's rule for this case gives the following results: for  $\Delta K = \pm 2$ ,  $\Delta \ell = -\frac{1}{2} \Delta K$ ; for  $\Delta K = \pm 1$ ,  $\Delta \ell = \Delta K$ ; and for  $\Delta K = 0$ , the rule cannot be satisfied. Therefore, the selection rules obeyed by degenerate fundamentals are  $\Delta K = \pm 2$  and  $\Delta K = \pm 1$  with the line strengths given by equations (2.16) and (2.15), respectively.

A doubly excited degenerate vibrational state transforms according to the symmetric direct product representation,  $\mathbf{E}\times\mathbf{E}=\mathbf{A}_1+\mathbf{E}, \text{ where } \mathbf{A}_1 \text{ and } \mathbf{E} \text{ refer to the parallel and}$ 

perpendicular components of the band, respectively (15). Therefore, none of the matrix elements  $<\tau, v|\mu_{\alpha}|\tau, v'>$ ,  $\mu_z$ ,  $\mu_z'$ , and  $\mu_x'$  are necessarily zero and  $\Delta K=0$ ,  $\pm 1$ ,  $\pm 2$  transitions are allowed. It must now be determined which  $\Delta K$  transitions take place to the E level and which take place to the  $A_1$  level as well as whether the intensities of the  $\Delta K=\pm 1$  transitions are given by either or both of equations (2.15) and (2.17) and whether the intensities of the  $\Delta K=0$  transitions are given by either or both of equations (2.14) and (2.16). A doubly excited degenerate vibrational state has vibrational angular momentum components of  $\ell=\pm 2$ , 0; the level that transforms according to E has  $\ell=\pm 2$  associated with it, while the level that transforms as  $A_1$  has  $\ell=0$  associated with it as shown in Figure (2.3).

symmetric 
$$E \times E = A_1 + E$$

$$A_1 & \ell = 0$$
Degenerate Vibrational State
$$A_2 & \ell = 0$$
Rovibronic Ground State

Figure 2.3 Symmetry of Doubly Excited Degenerate  $C_{3v}$  Vibration. The  $\Delta K=0$  transition can only occur between the ground rovibronic state and  $A_1$  state of the doubly excited degenerate vibrational state because Amat's rule required that  $\Delta L=0$  for  $\Delta K=0$ . Therefore the  $\Delta K=0$  transitions can only occur in the parallel component of the band with line strengths given by (2.14). The  $\Delta K=\pm 1$  transitions can only occur between the rovibronic ground state and the E state of the degenerate overtone because Amat's

rule requires that  $\Delta \mathcal{U} = \pm 2$  for  $\Delta K = \pm 1$ . Therefore, the line strengths of the  $\Delta K = \pm 1$  transition are given by equation (2.15). Finally, the  $\Delta K = \pm 2$  transitions from the ground state must terminate at the E level because Amat's rule requires  $\Delta \mathcal{U} = \pm 2$  for  $\Delta K = \pm 2$ .

The resulting selection rules are summarized in Table (2.3).

Type of vibration	ΔK	M	Transition moment given by equation	Line strength in Table
Non-degenerate fun- damentals and over- tones	∇K=0	∆€=∆K	(2.14)	2.4
Degenerate Funda- mentals	ΔK= <u>+</u> 1 ΔK= <u>+</u> 2	$\Delta \ell = \Delta K$ $\Delta \ell = -\frac{1}{2} \Delta K$	(2.15) (2.16)	2.5
Degenerate Overtones				
a. Parallel	<b>∇</b> K=0	Δε=ΔΚ	(2.14)	2.4
b. Perpendicular	ΔK= <u>+</u> 1 ΔK= <u>+</u> 2	Δε=-2ΔK Δε=ΔK	(2.15) (2.16)	2.5 2.6

E.F.S. selection rules for  $C_{3v}$  symmetry molecules.

 $\Delta J = 0$ ,  $\pm 1$ ,  $\pm 2$  in all cases.

Table (2.3)

#### LINEAR MOLECULES

The Sayvetz (18) conditions may be employed to specialize all of the expressions given for symmetric top molecules in this chapter to the case of linear polar molecules. For non-degenerate fundamentals and overtones of a linear molecule, the transition moment is given by equation (2.14) with K set equal to zero and the line strengths are given in Table (2.4) with K set equal to

#### TABLE (2.4)

# Line Strengths for $\Delta K=0$ Electric Field Induced Transitions

### A. Transitions Forbidden in Absence of Field

$$(|| \Gamma_{\mathbf{Z}})_{\mathbf{J}, \mathbf{K}, \tau, \mathbf{v}}^{\mathbf{J} = \mathbf{0}, \tau', \mathbf{v}'} = \frac{\mathbf{F}_{\mathbf{Z}}^{2}}{36} | \langle \tau, \mathbf{v} | \mu_{\mathbf{Z}} | \tau', \mathbf{v}' \rangle |^{2} \left| \frac{\mu_{\mathbf{Z}}}{hcB} + \frac{\mu'_{\mathbf{Z}}}{hcB'} \right|^{2}$$

$$(||f_{Z}||_{J,K_{F}\tau,V}^{J+2,K,\tau',V''}| = \frac{F_{Z}^{2}}{30}||c\tau,v||_{\mu_{Z}}||\tau',v'||^{2} \left|\frac{\mu'_{Z}}{hcB'(J+2)} - \frac{\mu_{Z}}{hcB(J+1)}\right|^{2}$$

$$\times \frac{[(J+1)^{2}-K^{2}][(J+2)^{2}-K^{2}]}{(J+1)(J+2)(2J+3)}$$

$$(\Pi \Gamma_{\mathbf{Z}}) \frac{J-2}{J,K,\tau,v}, v' = \frac{F_{\mathbf{Z}}^{2}}{30} | \langle \tau, v | \mu_{\mathbf{Z}} | \tau', v' \rangle |^{2} \left| \frac{\mu_{\mathbf{Z}}}{hcBJ} - \frac{\mu'_{\mathbf{Z}}}{hcB'(J-1)} \right|^{2}$$

$$\times \frac{(J^{2}-K^{2}) [(J-1)^{2}-K^{2}]}{J(J-1) (2J-1)}$$

$$(||\Gamma_X|)_{J,K,\tau,V}^{J=0,K=0,\tau',V'} = 0$$

$$(||\Gamma_X|)_{J,K,\tau,v}^{J+2,K,\tau',v'} = \frac{3}{4}(||\Gamma_Z|)_{J,K,\tau,v}^{J+2,K,\tau',v'}$$

$$(||\Gamma_X|) \frac{J-2,K,\tau',v'}{J,K,\tau',v'} = \frac{3}{4}(||\Gamma_Z|) \frac{J-2,K,\tau',v'}{J,K,\tau,v}$$

B. Correction to Transitions Allowed in Absence of Field

$$(\| \Gamma_{\mathbf{Z}}) \frac{J, K, \tau', v'}{J \neq 0, K, \tau, v} = \frac{F_{\mathbf{Z}}^{2} | \langle \tau, v | \mu_{\mathbf{Z}} | \tau', v' \rangle |^{2}}{60h^{2}c^{2}} \left[ \frac{\mu_{\mathbf{Z}}}{B} + \frac{\mu_{\mathbf{Z}}}{B'} \right]^{2}$$

$$\times \left[ \frac{(4J^{2}+1)(J^{2}-K^{2})}{J^{4}(2J-1)} - \frac{4(J^{2}-K^{2})[(J+1)^{2}-K^{2}]}{J^{2}(J+1)^{2}} + \frac{(4J^{2}+8J+5)[(J+1)^{2}-K^{2}]}{(J+1)^{4}(2J+3)} \right]$$

$$(\|\Gamma_{\mathbf{Z}})_{\mathbf{J},\mathbf{K},\tau,\mathbf{v}}^{\mathbf{J}+\mathbf{1},\mathbf{K},\tau',\mathbf{v}}^{\mathbf{I}',\mathbf{v}'} = \frac{\mathbf{F}_{\mathbf{Z}}^{2} |\langle \tau \mathbf{v} | \mu_{\mathbf{Z}} | \tau',\mathbf{v}' \rangle|^{2}}{60h^{2}c^{2}} \frac{\mathbf{J}(\mathbf{J}+2)K^{2} [(\mathbf{J}+1)^{2}-K^{2}]}{(\mathbf{J}+1)^{5}}$$

$$\times \left[ \frac{\mu_{\mathbf{Z}} - \mu_{\mathbf{Z}}^{2}}{2} \right]^{2}$$

$$x \left[ \frac{\mu_{z}}{B(J+2)} - \frac{\mu_{z}'}{B'J} \right]^{2}$$

$$(||\Gamma_{Z})_{J,K,\tau,v}^{J-1,K,\tau^{0}},v' = \frac{F_{Z}^{2} ||\tau||_{\mu_{Z}} ||\tau',v'||_{\mu_{Z}}^{2} ||\tau',v'||_{\mu_{Z}}^{2}$$

$$x \left[ \frac{\mu_z}{B(J-1)} - \frac{\mu_z}{B'(J+1)} \right]^2$$

$$(||\Gamma_{X}|_{J,K,\tau,v}^{J+1,K,\tau',v'}| = \frac{3}{4}(||\Gamma_{Z}|_{J,K,\tau,v}^{J+1,K,\tau',v'}$$

$$(||\Gamma_X|)_{J,K,\tau,v}^{J-1,K,\tau',v'} = \frac{3}{4}(||\Gamma_Z|)_{J,K,\tau,v}^{J+1,K,\tau',v'}$$

## TABLE (2.5)

## Line Strengths for $\Delta K = \frac{1}{2}l$ Electric Field Induced Transitions

## A. Transitions Forbidden in Absence of Field

$$(||\Gamma_{\mathbf{Z}})_{\mathbf{J},\mathbf{K},\tau,\mathbf{v}}^{\mathbf{J}+2,\mathbf{K}\pm1,\tau',\mathbf{v}'} = \frac{\mathbf{F}_{\mathbf{Z}}^{2}}{60}|\langle\tau,\mathbf{v}|\mu_{\mathbf{X}}|\tau',\mathbf{v}'\rangle|^{2} \left[\frac{\mu_{\mathbf{Z}}}{hcB(J+1)}\right] - \frac{\mu'_{\mathbf{Z}}}{hcB'(J+2)}^{2} \times \frac{[(J+1)^{2}-\mathbf{K}^{2}](J\pm\mathbf{K}+2)(J\pm\mathbf{K}+3)}{(J+1)(J+2)(2J+3)}$$

$$(||\Gamma_{Z})_{J,K,\tau,v}^{J-2,K^{\pm}1,\tau',v'} = \frac{F_{Z}^{2}}{60}|\langle\tau,v|\mu_{x}|\tau',v'\rangle|^{2} \left[\frac{\mu_{Z}}{hcBJ}\right] \times \frac{(J^{2}-K^{2})(J\mp K-1)(J\mp K-2)}{J(J-1)(2J-1)}$$

$$(||\Gamma_{X}|_{J,K,\tau,v}^{J+2,K\pm 1,\tau^*,v^*} = \frac{3}{4}(||\Gamma_{Z}|_{J,K,\tau,v}^{J+2,K\pm 1,\tau^*,v^*}$$

$$(||\Gamma_X|)_{J,K,\tau,v}^{J-2,K\pm 1,\tau',v'} = \frac{3}{4}(||\Gamma_Z|)_{J,K,\tau,v}^{J-2,K\pm 1,\tau',v'}$$

## B. Corrections to Transitions Allowed in Absence of Field

$$(||f_{Z}) \frac{J \neq 0, K \pm 1, \tau', v'}{J, K, \tau, v} = \frac{F_{Z}^{2}}{120} ||c\tau, v||_{\mu_{X}} ||\tau', v'| > ||^{2} \frac{(J \mp K) (J \pm K + 1)}{(2J + 1)}$$

$$\times \frac{(4J^{2} + 1)}{J^{5} (2J - 1)} ||\frac{\mu_{Z}}{hcB} (J \pm K)| - \frac{\mu'_{Z}}{hcB'} (J \mp K - 1) ||^{2}$$

$$+ \frac{4}{J^{2} (J + 1)^{2}} ||\frac{\mu_{Z}}{hcB} (J \pm K)| - \frac{\mu'_{Z}}{hcB'} (J \mp K - 1) ||\frac{\mu_{Z}}{hcB} (J \mp K + 1)|$$

$$- \frac{\mu'_{Z}}{hcB'} (J \pm K + 2) || + \frac{(4J^{2} + 8J + 5)}{(J + 1)^{5} (2J + 3)} ||\frac{\mu_{Z}}{hcB} (J \mp K + 1) - \frac{\mu'_{Z}}{hcB'} (J \pm K + 2) ||^{2}$$

$$(\|\Gamma_{\mathbf{Z}})_{\mathbf{J},\mathbf{K},\tau,\mathbf{v}}^{\mathbf{J}+\mathbf{1},\mathbf{K}\pm\mathbf{1},\tau',\mathbf{v}'} = \frac{\mathbf{F}_{\mathbf{Z}}^{2}}{120 \ h^{2}c^{2}} | \langle \tau,\mathbf{v} | \mu_{\mathbf{X}} | \tau',\mathbf{v}' \rangle |^{2} \frac{\mathbf{J}(\mathbf{J}+\mathbf{2})}{(\mathbf{J}+\mathbf{1})^{5}}$$

$$\mathbf{x} \left[ \frac{\mu_{\mathbf{Z}}(\mathbf{J}\mp\mathbf{K}+\mathbf{1})}{\mathbf{B}(\mathbf{J}+\mathbf{2})} - \frac{\mu'_{\mathbf{Z}}(\mathbf{J}\mp\mathbf{K})}{\mathbf{B}'\mathbf{J}} \right]^{2}$$

 $x (J\pm K+1) (J\pm K+2)$ 

 $x (J \mp K) (J \mp K - 1)$ 

$$(||f_{\mathbf{Z}}||_{\mathbf{J},K,\tau,\mathbf{V}}^{\mathbf{J-1},K\pm 1,\tau',\mathbf{V'}} = \frac{|f_{\mathbf{Z}}|^{2}}{120 |h^{2}c^{2}} ||f_{\mathbf{V}}||_{\mathbf{X}} ||f_{\mathbf{V}}||_{\mathbf{X}} ||f_{\mathbf{V}}||_{\mathbf{Z}} \frac{(J+1) (J-1)}{J^{5}}$$

$$\times \left[ \frac{|h_{\mathbf{Z}}|(J\pm K)|}{B(J-1)} - \frac{|h_{\mathbf{Z}}|^{2} (J\pm K+1)}{B^{2} (J+1)} \right]^{2}$$

$$\begin{aligned} (\|\Gamma_{K})_{J,K,\tau,v}^{J\neq0,K^{\pm}1,\tau',v'}^{\pm 1,\tau',v'} &= \frac{F_{Z}^{2}}{240 \ h^{2}c^{2}} | <\tau,v | \mu_{X} | \tau',v'> |^{2} \\ &= \frac{J(J+1) \ (J^{\pm}K) \ (J^{\pm}K+1)}{(2J+1)} \times \left\{ \frac{1}{J^{6} \ (2J-1)} \left[ \frac{\mu_{Z}^{2}}{B^{2}} (J^{\pm}K)^{2} (6J-1) \right] \right. \\ &+ \frac{8\mu_{Z}\mu'_{Z}}{BB'} (J^{\pm}K-1) \ (J^{\pm}K) \ (J-1) + \frac{\mu'_{Z}^{2}}{B'^{2}} (J^{\pm}K-1)^{2} (6J-1) \right] \\ &- \frac{2}{J^{2} \ (J+1)^{2}} \frac{2\mu_{Z}^{2}}{B^{2}} (J^{\pm}K) \ (J^{\pm}K+1) + \frac{3\mu_{Z}\mu'_{Z}}{BB'} (2J^{2}+2J-1+2K^{2}\pm2K) \\ &+ \frac{2\mu'_{Z}^{2}}{B'^{2}} (J^{\pm}K-1) \ (J^{\pm}K+2) \right] \\ &+ \frac{1}{(J+1)^{6} \ (2J+3)} \left[ \frac{\mu_{Z}^{2}}{B^{2}} (J^{\pm}K+1)^{2} \ (6J+7) + \frac{8\mu_{Z}\mu'_{Z}}{BB'} (J^{\pm}K+1) (J^{\pm}K+2) (J+2) \right. \\ &+ \frac{\mu'_{Z}^{2}}{B'^{2}} (J^{\pm}K+2)^{2} \ (6J+7) \right] \right\} \end{aligned}$$

$$(||\Gamma_X|_{J,K,\tau,v}^{J-1,K\pm 1,\tau',v'}| = \frac{3}{4}(||\Gamma_Z|_{J,K,\tau,v}^{J+1,K\pm 1,\tau',v}|)$$

$$(||\Gamma_X|)_{J,K,\tau,v}^{J-1,K\pm 1,\tau',v'} = \frac{3}{4}(||\Gamma_Z|)_{J,K,\tau,v}^{J-1,K\pm 1,\tau',v}$$

## TABLE (2.6)

# Line Strengths for $\Delta K=\pm 2$ Electric Field Induced Transitions

$$\begin{array}{l}
\coprod_{Z} J_{J,K,\tau,v} = \frac{F_{Z}^{2} | < \tau, v | \mu_{X} | \tau', v' > |^{2} (J + K) (J + K - 1)}{240 h^{2} c^{2}} \\
(J + K + 1) (J + K + 2) \times \left\{ \frac{(4J^{2} + 1)}{J^{3} (2J - 1)} \left[ \frac{\mu_{X}}{2BJ - (A - B) (1 \pm 2K)} \right] \right. \\
+ \frac{\mu'_{X}}{2B'J + (A' - B') (3 \pm 2K)} \right]^{2} - \frac{4}{J(J + 1)} \left[ \frac{\mu_{X}}{2BJ - (A - B) (1 \pm 2K)} \right] \\
+ \frac{\mu'_{X}}{2B'J + (A' - B') (3 \pm 2K)} \times \left[ \frac{\mu_{X}}{2B(J + 1) + (A - B) (1 \pm 2K)} \right] \\
+ \frac{\mu'_{X}}{2B'(J + 1) - (A' - B') (3 \pm 2K)} + \frac{(4J^{2} + 8J + 5)}{(J + 1)^{3} (2J + 3)} \right] \\
\left[ \frac{\mu_{X}}{2B(J + 1) + (A - B) (1 \pm 2K)} + \frac{\mu'_{X}}{2B'(J + 1) - (A' - B') (3 \pm 2K)} \right]^{2} \\
( \perp \Gamma_{Z}) J_{J,K,\tau,v}^{3J + 1, K \pm 2, \tau', v'} = \frac{F_{Z}^{2}}{60 h^{2} c^{2}} | \tau', v | \mu_{X} | \tau', v' > |^{2} \frac{J(J + 2)}{(J + 1)^{3}} \\
\times \left[ \frac{\mu_{X}}{[2B(J + 1) + (A - B) (1 \pm 2K)] (J + 2)} - \frac{\mu'_{X}}{[2B'(J + 1) + (A' - B') (3 \pm 2K)] J} \right]^{2}
\end{array}$$

x (J $\mp$ K) (J $\pm$ K+1) (J $\pm$ K+2) (J $\pm$ K+3)

$$(\mathbf{L}_{\mathbf{Z}})_{\mathbf{J},\mathbf{K},\mathbf{v},\mathbf{v}}^{\mathbf{J}-\mathbf{1},\mathbf{K}+2,\mathbf{v}',\mathbf{v}'} = \frac{\mathbf{F}_{\mathbf{Z}}^{2}}{60 \ h^{2}c^{2}} |\langle \mathbf{v},\mathbf{v} | \mu_{\mathbf{X}} | \mathbf{\tau}',\mathbf{v}' \rangle|^{2} \frac{(\mathbf{J}+\mathbf{1}) (\mathbf{J}-\mathbf{1})}{\mathbf{J}^{3}}$$

$$x \left[ \frac{\mu_{x}}{[2BJ-(A-B)(1\pm2K)](J-1)} - \frac{\mu_{x}}{[2B'J-(A'-B')(3\pm2K)](J+1)} \right]^{2}$$

 $x (J \mp K) (J \mp K - 1) (J \mp K + 1) (J \mp K - 2)$ 

$$(\mathbf{1}\Gamma_{\mathbf{Z}})\frac{J+2,K\pm2,\tau',v'}{J,K,\tau,v} = \frac{\mathbf{F}_{\mathbf{Z}}^{2}}{30 \ h^{2}c^{2}} | \langle \tau,v | \mu_{\mathbf{X}} | \tau',v' \rangle |^{2}$$

$$\times \left[ \frac{\mu_{\mathbf{X}}}{2B(J+1)+(A-B)(1\pm2K)} - \frac{\mu'_{\mathbf{X}}}{2B'(J+2)+(A'-B')(3\pm2K)} \right]^{2}$$

$$\times \frac{(J^{\pm}K+1) (J^{\pm}K+2) (J^{\pm}K+3) (J^{\pm}K+4)}{(J+1) (J+2) (2J+3)}$$

$$(\perp \Gamma_{z})_{J,K,\tau,v}^{J-2,K\pm2,\tau',v'} = \frac{F_{z}^{2}}{30 h^{2}c^{2}} | \langle \tau, v | \mu_{x} | \tau', v' \rangle |^{2}$$

$$x \left[ \frac{\mu_{x}}{2BJ - (A-B)(1\pm 2K)} - \frac{\mu'_{x}}{2B'(J-1) - (A'-B')(3\pm 2K)} \right]^{2}$$

$$\times \frac{(J\mp K) (J\mp K-1) (J\mp K-2) (J\mp K-3)}{J (J-1) (2J+1)}$$

$$( \pm \Gamma_{X}) \frac{J \ge 2, K \pm 2, \tau', v'}{J, K, \tau, v} = \frac{F_{Z}^{2} | \langle \tau, v | \mu_{X} | \tau', v' \rangle |^{2}}{120 h^{2}c^{2}}$$

$$( J \pm K + 1) ( J \pm K + 2) \times \begin{cases} \frac{J(J+1)}{(2J+1)} & \frac{1}{J^{*}(2J-1)} \end{cases} p^{2} (6J-1) - 8pq(J-1)$$

$$+ q^{2}(6J-1) + \frac{2}{J^{2}(J+1)^{2}} \left[ 2ps - 3(pt + qs) + 2qt \right]$$

$$+ \frac{1}{(J+1)^{4}(2J+3)} \left| s^{2}(6J+7) - 8st(J+2) + t^{2}(6J+7) \right|$$

where

$$p = \frac{\mu_{x}}{2BJ - (A - B) (1 \pm 2K)}$$

$$q = \frac{\mu'_{x}}{2B'J + (A' - B') (3 \pm 2K)}$$

$$s = \frac{\mu_{x}}{2B(J + 1) + (A - B) (1 \pm 2K)}$$

$$t = \frac{\mu_{x}'_{x}}{2B'(J + 1) - (A' - B') (3 \pm 2K)}$$

$$(\bot\Gamma_{\rm X})_{{\rm J},{\rm K},\tau,{\rm v}}^{{\rm J}+1,{\rm K}\pm2,\tau',{\rm v'}} = \tfrac{3}{4}(\bot\Gamma_{\rm Z})_{{\rm J},{\rm K},\tau,{\rm v}}^{{\rm J}+1,{\rm K}\pm2,\tau',{\rm v'}}$$

$$(\perp \Gamma_{X})_{J,K,\tau,v}^{J-1,K\pm 2,\tau',v'} = \frac{3}{4}(\perp \Gamma_{Z})_{J,K,\tau,v}^{J-1,K\pm 2,\tau',v'}$$

$$(\perp \Gamma_X)_{J,K,\tau,v}^{J+2,K\pm2,\tau',v'} = \frac{3}{4}(\perp \Gamma_Z)_{J,K,\tau,v}^{J+2,K\pm2,\tau',v'}$$

$$(\perp^{\Gamma}_{X})_{J,K,\tau,v}^{J-2,K\pm2,\tau',v'} = \frac{3}{4}(\perp^{\Gamma}_{Z})_{J,K,\tau,v}^{J-2,K\pm2,\tau',v'}$$

zero. Transitions involving the degenerate vibrational states of linear molecules cannot be treated by the above non-degenerate perturbation theory because degenerate states with the same  $\pm \ell$  within the same vibrational state interact through the electric field. Degenerate perturbation theory is applied to this problem in Chapter IV in connection with the interpretation of observed electric field induced spectra of HCN.

#### LINE SHAPES

The following development of the theory of electric field induced spectra by Bridge, Haner, and Dows (13) parallels the perturbation treatment already presented and gives additional information on expected line shapes.

In the absence of an external field absorption line shapes are due to three processes. First, the natural line breadth results from the finite lifetime of energy states in conjunction with the uncertainty principle. Secondly, the random motion of molecules in a gas causes absorption of a distribution of frequencies due to the Doppler effect that can be described by a Gaussian function. Finally, interactions between molecules— pressure broadening—causes absorption with a Lorentzian distribution of frequencies.

In addition, an external electric field removes the upper and lower state M degeneracies and even though the transitions may not be resolvable, a distribution of frequencies about the central frequency will be present. We will characterize electric field induced absorption lines by their center frequency, an integrated line strength, and a line shape that arises from the

field splittings in addition to the other broadening effects described above.

Assuming a line shape function S and retaining the previous weak field assumption so that the absorption coefficient  $k(\nu)$  is a sum over the upper and lower state M degeneracies, the absorption coefficient becomes

$$k(v_z F_z) = [hv_{JK}/(2J+1)] \sum_{M,M'} B_{JKM}(F_z)S[v - v_{0JKM}(F_z)],$$
 (2.20)

where the only previously undefined symbol is  $\nu_{\rm OJKM}$ , the frequency of the absorption line including field effects. The form of S can be taken as independent of M so long as the assumption of weak electric fields is valid.

Under the assumption of weak fields the absorption coefficient  $k(\nu,F_Z) \quad \text{and the Einstein} \quad B \quad \text{coefficient may each be expanded in}$  powers of the field.

$$k(v,F_Z) = k_0(v) + F_Z^2 k_2(v) + F_Z^4 k_4(v) + \dots$$
 (2.21)

$$B_{JKM}(F_Z) = B_{OJKM} + F_Z B_{1JKM} + F_Z^2 B_{2JKM} + \dots$$
 (2.22)

Odd powers of the field drop out of the absorption coefficient  $k(\nu,F_{\rm Z}) \ \ \text{on summing over} \ \ M \ \ and \ \ M' \ \ because$ 

$$A_{nJKMJ'K'M'}F_Z^n = A_{nJK-MJ'K'M'}(-F_Z)^n.$$

This is apparent because absorption cannot depend upon the sense of the field. The  $B_{OJKM}$  in (2.22) are the field independent Einstein B coefficients for induced absorption and the  $B_{2JKM}$  are proportional (by a factor of  $8\pi^3/\text{hc}$ ) to the  $(\Gamma)_{JKM}^{J'K'M'}$  calculated earlier. The  $B_{1JKM}$  are discussed qualitatively below. A similar

expansion of the frequency  $\nu_{0JKM}^{(F)}$  occurring in the argument of the line shape function yields:

$$v_{0JKM}(F_Z) = v_{0JKM}^0 + f_{1JKM}F_Z + f_{2JKM}F_Z^2 + \dots,$$
 (2.23)

where  $f_{nJKM}$  are the  $n\frac{th}{t}$  order Stark splittings.

If the Stark frequency shifts are small compared to the line width  $\Delta$ , the line shape function can be expanded in powers of the shift.

$$S\{v - v_{OJKM}(F_Z)\} = S\{v - v_o^o\} + S^{I}\{v - v_o^o\}[v - v_o]/\Delta$$

$$+ S^{II}\{v - v_o^o\}[(v - v_o)/\Delta]^2 + \dots, \qquad (2.24)$$

where the coefficients  $S^{n}(v)$  are, by Taylor's theorem,

$$S^{n}(v) = (-\Delta)^{n}(n!)^{-1} \frac{d^{n}}{dv^{n}} S(v) .$$

Combining expansions (2.22), (2.23), and (2.24) and comparing coefficients of  $\mathbb{F}^n_Z$  with expansion (2.21) makes the following identifications possible.

$$k_{o}(v) = [hv_{JK}/(2J+1)]_{MM}^{2} B_{OJKM} S\{v - v_{o}^{o}\}$$

$$k_{2}(v) = [hv_{JK}/(2J+1)]_{MM}^{2} B_{OJKM}(f_{1}/\Delta)^{2} S^{II}\{v - v_{o}^{o}\}$$

$$+ \frac{[B_{OJKM}(f_{2}/\Delta) + B_{1JKM}(f_{1}/\Delta)]S^{I}\{v - v_{o}^{o}\}}{MM}^{2} B_{OJKM}(f_{2}/\Delta) + B_{1JKM}(f_{1}/\Delta)^{2} S^{I}\{v - v_{o}^{o}\}$$

$$+ \frac{B_{2JKM}}{MM} S\{v - v_{o}^{o}\}$$

$$k_{4}(v) = [hv_{JK}/(2J+1)]_{MM}^{2} [B_{o}(f_{1}/\Delta)^{4} S^{IV}\{v - v_{o}^{o}\} + \dots]. \qquad (2.25)$$

 $k_{2}(v)$  in equation (2.25) is made up of three terms:

$$k_2(v) = k_2^a(v) + k_2^b(v) + k_2^c(v)$$
, (2.26)

where

$$k_2^a(v) = \int hv_{JK}/(2J+1) \int_{MM'}^{L} B_{2JKM} S\{v - v_o^o\}$$

$$k_2^b(v) = \left[hv_{JK}/(2J+1)\right] \sum_{MM} \left[B_{0JKM}(f_2/\Delta) + B_{1JKM}(f_1/\Delta)\right] S^{I} \left\{v - v_0^{o}\right\}$$

$$k_2^c(v) = [hv_{JK}/(2J+1)]_{MM}^2 B_{0JKM}(f_1/\Delta)^2 S^{II}\{v - v_0^c\}$$

These three terms correspond to three different types of electric field induced spectra (EFS)-type (a) EFS in which  $k_2^a$  dominates the other two terms, type (b) EFS when  $k_2^b$  dominates the other two terms, and type (c) EFS when  $k_2^c$  dominates  $k_2^a$  and  $k_2^b$ . The type of EFS observed is determined by the molecular parameters involved rather than being the choice of the experimenter.

 $k_2^a(v)$  is the absorption coefficient of a line having the same shape  $S(v-v_0^0)$  as an absorption line in the absence of the field but a different line strength  $B_{2JKM}$ . Therefore, a type (a) EFS difference spectrum will be a spectrum showing the same line shapes as a field free absorption spectrum but with a different intensity distribution and different selection rules. The line strengths of type (a) EFS are those calculated previously in the chapter, given in Tables 2.4 through 2.6.

 $k_2^D(v)$  contains two terms - one involving first order Stark splitting  $f_1$  and the other involving second order Stark splitting  $f_2$ . The second order Stark effect term has the same line strength

as a field-free absorption line so a type (b) EFS difference spectrum will appear as the difference between two lines of the same intensity, one slightly shifted in frequency from the other due to second order Stark splitting. The first order Stark effect term describes the fact that some intensity is transferred from the  $M \rightarrow M'$  transition to the  $-M \rightarrow -M'$  transition. I have not calculated the  $B_{1\,\mathrm{IVM}}$ .

 $k_2^c(v)$  is directly interpretable in terms of the first order Stark effect. A type (c) EFS difference spectrum will appear as the difference between two absorption lines of the same strength  $B_{OJKM}$  one of which is broadened with respect to the other by first order Stark splitting. The line strengths for  $k_2^c(v)$  have been calculated for perpendicular bands (13) and are given in Table (2.7).

If the line shape is assumed Lorentzian, then the three line shapes are (from Taylor's theorem):

type (a) EFS

$$S\{v - v_o^o\} = (1/\pi\Delta)(1/(x^2 + 1)),$$
 (2.27)

type (b) EFS

$$S^{I}\{\nu - \nu_{o}^{\circ}\} = (1/\pi\Delta) \left\{ \frac{2x}{(x^{2} + 1)^{2}} \right\},$$
 (2.28)

type (c) EFS

$$S^{II}\{\nu - \nu_o^o\} = (1/\pi\Delta)((3x^2 - 1)/(x^2 + 1)^3), \qquad (2.29)$$

where  $x = (v - v_0^0)/\Delta$ .

These are shown graphically in Figure (2.4) and are in agreement

## TABLE 2.7

## Line Strengths of EFS Type (c) Transitions

## A. Light Polarized Parallel to the Electric Field

Transition

Line Strength

$$J \to J + 1 \qquad \frac{\left| <\tau, v \middle| \mu_{x} \middle| \tau', v' > \right|^{2} J(J + 2) (J + K + 1) (J + K + 2)}{60h^{2}c^{2}\Delta^{2} (2J + 1) (J + 1)^{3}} \times \left\{ \frac{(K + 1)\mu'_{z}}{J + 2} - \frac{K \mu_{z}}{J} \right\}^{2}$$

$$J \to J \qquad \frac{\left| <\tau, v \middle| \mu_{x} \middle| \tau', v' > \right|^{2} (3J^{2} + 3J - 1) \left[ J(J + 1) - K(K + 1) \right]}{60h^{2}c^{2}\Delta^{2}J^{3}(J + 1)^{2}(2J + 1)}$$

$$\times \left\{ (K \pm 1)\mu'_{z} - K \mu_{z} \right\}^{2}$$

$$J \to J - 1 \qquad \frac{\left| \langle \tau, v | \mu_{x} | \tau', v' \rangle \right|^{2} (J^{2} - 1) (J + K) (J + K - 1)}{60h^{2}c^{2}\Delta^{2} J^{3} (2J + 1)}$$

$$\times \left\{ \frac{(K \pm 1)\mu^{2}}{J-1} - \frac{K \mu_{z}}{J+1} \right\}^{2}$$

## B. Light Polarized Perpendicular to the Electric Field

Transition Line Strength  $\frac{\left| \langle \tau, v | \mu_{x} | \tau^{x}, v^{z} \rangle \right|^{2} (J \pm K + 1) (J \pm K + 2)}{120h^{2}c^{2}\Delta^{2} (J + 1)^{3} (2J + 1)}$ K → K ± 1  $\times \left\{ \frac{4J + 5}{J + 2} (K + 1)^{2} \mu_{z}^{2} - 8K(K + 1) \mu_{z} \mu_{z}^{2} \right\}$  $+\frac{4J+3}{J} \kappa^2 \mu_z^2$  $\frac{\left|\langle \tau, v | \mu_{x} | \tau', v' \rangle \right|^{2} \left[ J(J+1) - K(K+1) \right]}{120h^{2}c^{2}h^{2}J^{3}(2J+1)(J+1)^{2}}$ J → J  $K \rightarrow K \pm 1$  $\times \left\{ (2J^2 + 2J + 1)[(K \pm 1)\mu_z' - K \mu_z]^2 \right\}$  $+ 10 \text{ K}(\text{K} \pm 1)\mu_z\mu_z^{\dagger}$  $\frac{\left| <\tau, v | \mu_{x} | \tau', v' > \right|^{2} (J + K) (J + K - 1)}{120h^{2}c^{2}\Delta^{2} J^{3} (2J + 1)}$  $J \rightarrow J - 1$  $K \rightarrow K + 1$  $\times \left\{ \frac{4J - 1}{J - 1} (K \pm 1)^{2} \mu_{z}^{2} - 8K(K \pm 1) \mu_{z} \mu_{z}^{2} \right\}$  $+\frac{4J+1}{J+1}K^{2}_{\mu z}$ 

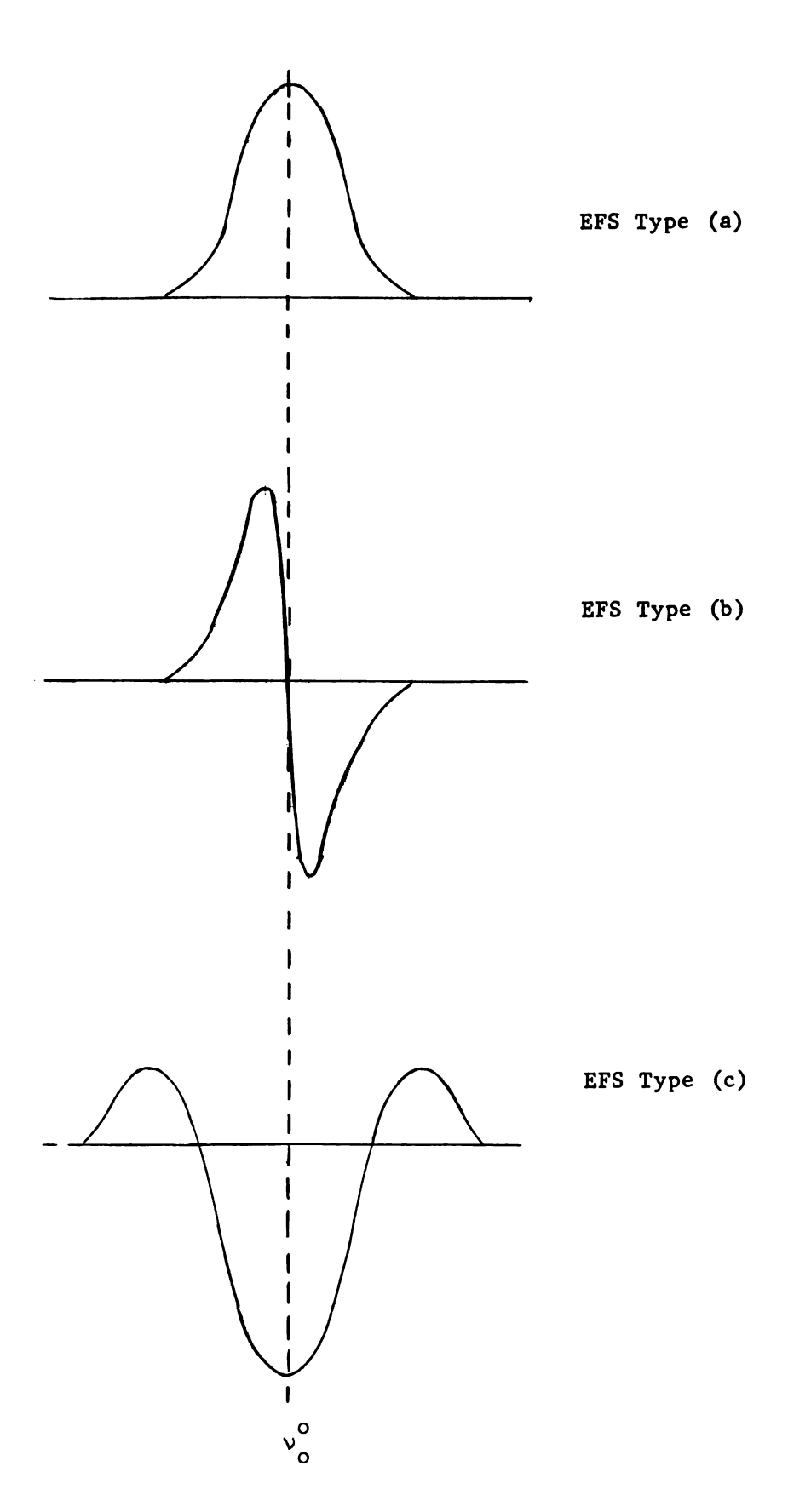


Figure (2.4) Electric Field Induced Line Shapes.

with the qualitative arguments presented above.

In practice, the line shape function is a much more complicated function than Lorentzian or Gaussian (c.f., 19 or 20) and monochromator slit effects must be considered. The intensity of the absorption line is transformed by the spectrometer according to

$$I'(v',F_Z) = \int I(v,F_Z)\beta(v - v')dv, \qquad (2.30)$$

where the slit function  $\beta(\nu - \nu')$  is the fractional intensity of light of frequency  $\nu$  transmitted by the spectrometer set to frequency  $\nu'$  and  $I(\nu,F_Z)$  is given for a Beer's law absorber by

$$I(v,F_Z) = I^{\circ}(v) \exp \left[-k(v,F_Z)L\right], \qquad (2.31)$$

where L is the absorption path length and  $I^{O}(v)$  is the intensity of the incident radiation of frequency v.

#### VALIDITY OF PERTURBATION EXPANSION

The perturbation and power series expansion treatments of electric field induced spectra both require the perturbing field to be weak. This requirement means that the perturbation energy  $\mu F$  must be small compared to the separation of rotational energy levels, i.e., for a polar axially symmetric molecule  $\mu F < 2hcBJ$  for the  $J^{\frac{th}{T}}$  rotational level, B being the rotational constant in units of cm<sup>-1</sup>. For methyl fluoride with  $\mu \cong 2$  Debye and  $B \cong 1$  cm<sup>-1</sup>, the upper limit on the field is 200J esu (60J KV/cm) so that a field of 30 Kv/cm is small for practically all rotational levels.

For high electric fields and in the case of molecules possessing large electric dipole moments, the perturbation expansion does not converge. In these cases, Lamb's method (see Chapter I) of finding an exact solution for the Stark energy levels could be used. With very accurate values of Stark energy changes, accurate numerical wave functions good for all values of electric field could be found for use in intensity calculations. A considerable amount of computer time and storage space would be required for this problem in all cases except for very low values of J.

#### CHAPTER III

## EXPERIMENTAL TECHNIQUE

The apparatus and frequency measuring techniques used in the experimental portion of this thesis are described in this chapter.

Two experimental stages for the detection and measurement of electric field induced spectra were used in the course of this work. The original system was assembled to determine whether EFS could be observed in the near infrared region. As soon as induced spectra were obtained using the original system, improvements were made in the design of the fore-optical system to increase energy and improve resolution. Both experimental arrangements are described below.

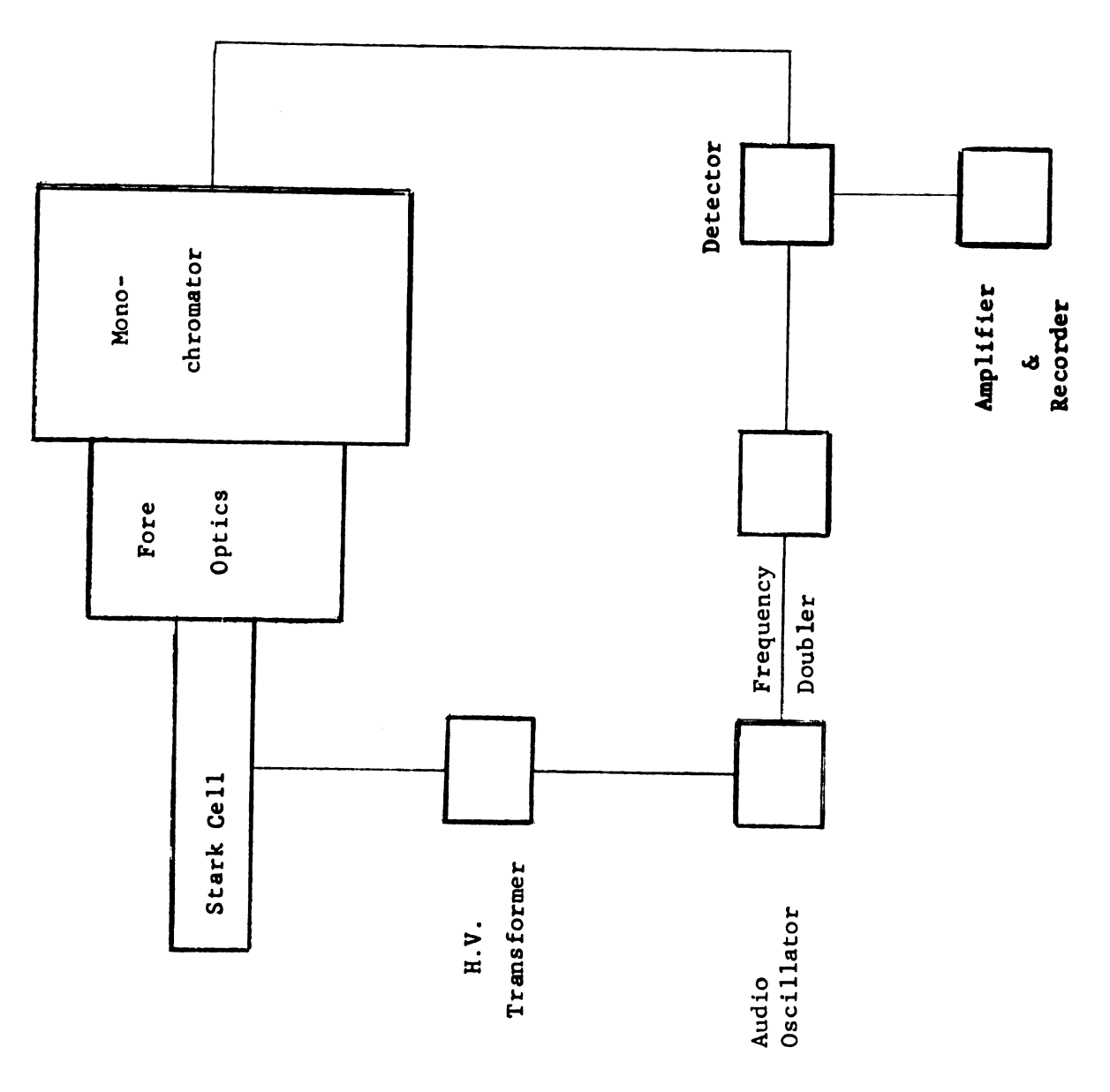
Because induced intensity changes are proportional to the square of the electric field and are orders of magnitude smaller than zero-field absorption signals, it was decided to use phase sensitive ac electronic techniques. An ac electric field was used to modulate the light transmitted by the cell (rather than a mechanical light chopper) and amplification was done at twice the electric field frequency because of the  $F_Z^{\ 2}$  dependence of the line strength.

A block diagram of the apparatus is shown in Figure (3.1).

The general experimental arrangement was the following.

Light from the carbon rod source (21) was focused by a CaF<sub>2</sub> lens at the entrance of the parallel plate, electrically capacitive,

"Stark cell" described in detail below. The light was modulated



Lens

Source

Figure (3.1) General BFS Experimental Arrangement

by the 45 Hz. high voltage applied to the hot electrode of the Stark cell and then focused by fore optics on the entrance slit of the monochromator (described in detail by Aubel (22) with modifications described by Keck (21)). The dispersed light from the monochromator was then focused on a lead sulfide detector cooled to liquid nitrogen temperature. The signal from the lead sulfide detector was phase sensitive detected (Aubel (22)) using a 90 Hz. reference signal, amplified, and finally recorded by one pen of a Leeds and Northrup dual pen recorder. Electrical energy for the high voltage and the reference signal was provided by a Behlman Engineering audio oscillator having three 120 volt outputs. The 45 Hz. reference voltage had its frequency doubled by a lab built full wave rectifier and was fed into the phase sensitive detector through a phase shifting network providing phase changes throughout 360 degrees.

## INITIAL EXPERIMENT

Because electric field induced signals are small, Stark cell design is important. In order to observe induced transitions, the cell must provide electric fields of the order of tens of Kv/cm, transmit a reasonable fraction of incident radiation, and provide an absorption path length sizable enough for appreciable absorption to occur. Professor C. W. Peter's group at the University of Michigan faced identical problems in their Stark effect experiments and our cell is essentially a copy of theirs (5).

The original Stark cell was constructed as shown in Figure (3.2). Two slabs, 2"x36"x½", of selected Libbey Ownes Ford 'Mirro-Pane', a front surface chromium coated mirror, were separated by ½" wide .0075" strips of insulating Du Pont 'Mylar' and stainless

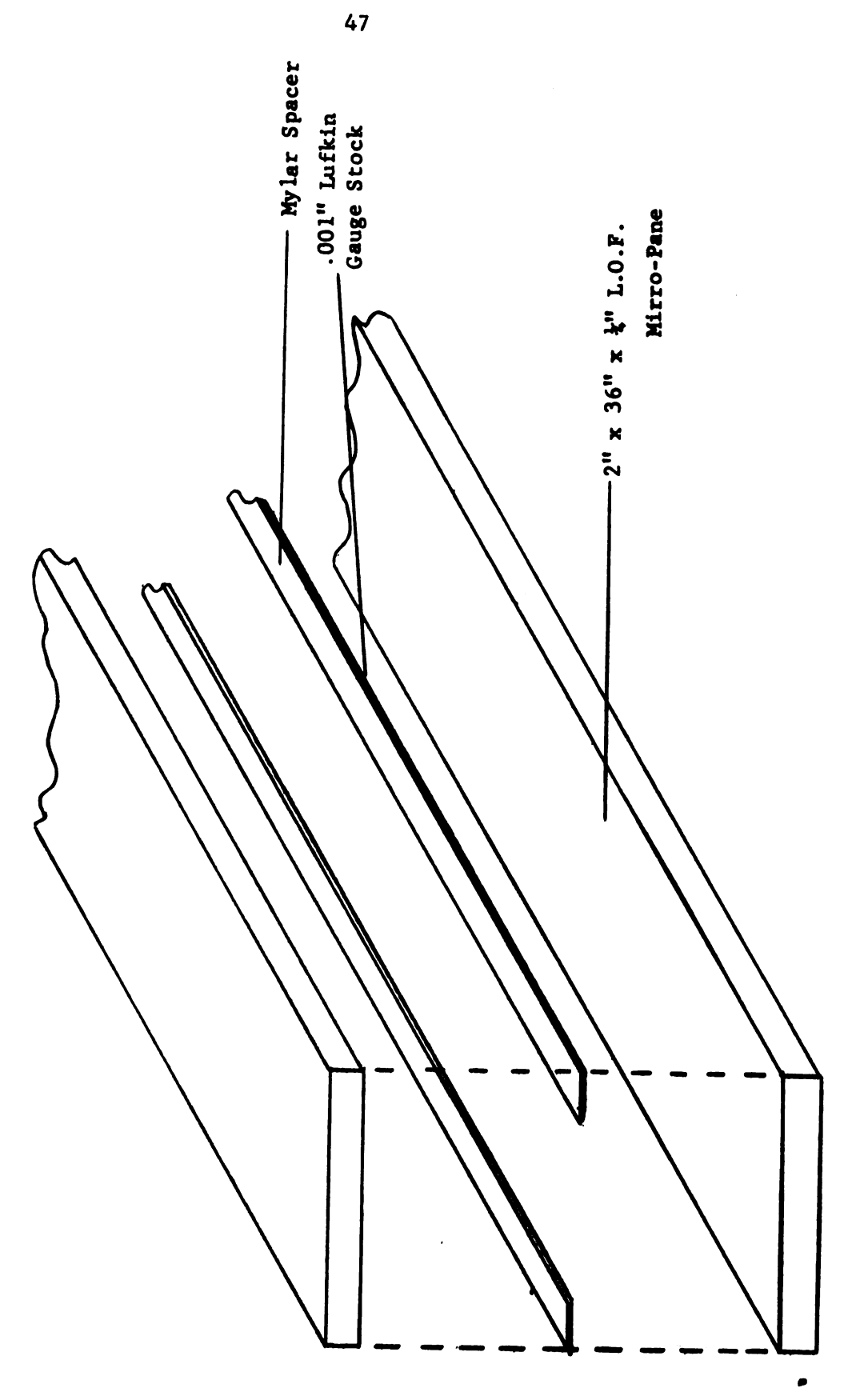


Figure (3.2) Stark Cell

steel Lufkin gauge stock. The gauge stock also served to make electrical contact to the mirror surfaces. With the spacers in place, the cell was placed between two pieces of channel iron loaded with lead bricks. Pressure was uniformly distributed along the edges of the cell by placing rubber strips between the glass and the iron rails. Ren Plastics RP 201 green epoxy was used to cement along the edges. Later cells were cemented with RP 1240 because it is easier to handle. The cell was placed in a housing consisting of a piece of brass S band wave guide with removable endplates and CaF, end windows. Sample pressures were measured by a Welch Scientific Co. Dubrovin gauge connected to the housing through a glass manifold. The manifold also served to introduce and remove sample gases from the Stark cell. One electrode lead (gauge stock) was soldered directly to the grounded brass housing. The high voltage was connected to the cell through a hermetic seal. The exposed gauge stock was covered with corona dope to prevent electrical breakdown of the gas at these places. The brass housing and accessories remained basically unchanged throughout the experimental portion of this work. All six Stark cells constructed during this portion of the work suffered electrical breakdown after five to eight hours of operation and had to be discarded.

In the first system, a 12 cm focal length CaF<sub>2</sub> lens was used to form an image of the exit aperture of the Stark cell at an intermediate focus of the monochromator. Because the optical elements used in the preliminary investigation were those on hand in the laboratory, matching the f/ number of the light beam to the monochromator was impossible. Weak but interesting electric field

induced transitions in CH<sub>3</sub>Br, CH<sub>3</sub>I, and CH<sub>3</sub>CN were observed with this apparatus although no frequency measurements were attempted at that time.

#### FINAL ARRANGEMENT

The largest defect in the original experiment was the lack of energy available in the monochromator. In order to overcome this difficulty, it was decided to increase the separation of the Stark cell plates to about 2 mm. as a method of increasing transmission efficiency and make a careful study of the optical properties of such a cell to see if it could be conveniently matched to the monochromator. However, wider separation of the plates decreases the breakdown voltage of a gas at low sample pressures; but this problem can be minimized with a heavy inert buffer gas such as SF<sub>6</sub> (23). Essentially, this is a trade of possible resolution, because of the pressure broadening, for energy in the monochromator.

It was observed experimentally with plate separations on the order of 2 mm. that light diverged horizontally from the <u>exit</u> end of the Stark cell at approximately f/8 and diverged vertically from the <u>entrance</u> end of the cell at approximately f/20 using f/4 source optics. The horizontal f/ number was not well defined. The beam was observed to have a non-uniform intensity distribution in the horizontal plane due to multiple reflections from the cell walls. The appearance of the pattern resembled an interference pattern with poorly defined edges and was highly dependent upon alignment.

The optical problem was to fill the monochromator, correcting for the astigmatism (equal to the length of the cell), and simultaneously match both horizontal and vertical f/ numbers to that of the monochromator.

My solution to this problem for a Stark cell of arbitrary length L is the following two lens system. A spherical lens placed at its focal distance from the exit end of the cell to simultaneously match the vertical f/ number of the cell to the monochromator and collimate the horizontally divergent portion of the bean. With these two conditions plus the fact that the difference between the object distances for the horizontal and vertical portions of the beam is the length of the cell L, the required focal length f of the spherical lens may be calculated from the thin lens formula as

f = mL.

m is the ratio of the f/ number of the monochromator to the cell's vertical f/ number, viz., the magnification required to match the cell's vertical f/ number to that of the monochromator. The second lens, beyond the spherical lens, is cylindrical with an f/ number equal to that of the monochromator and a focal length determined by the width of the collimated beam. The cylindrical lens, while having little effect on the vertical portion of the beam, focuses the collimated protion of the beam at the point where the spherical lens focused the vertical portion of the beam.

Although our monochromator is f/5, it was more convenient to focus the emergenent light at an intermediate focus in the regular fore-optical system at f/10. The 100 cm length of our Stark cell and the demagnification of the vertical portion of the beam from

f/20 to f/10 determined the focal length of the spherical lens to be 50 cm. The measured horizontal dimension of 6.5 cm, together with the required f/10, of the collimated beam determined the focal length of the cylindrical lens to be 65 cm. The optical system is shown in Figure (3.3).

Details of the shape calculations for the two CaF  $_{\rm 2}$  lenses used in this system are presented below.

#### LENS CALCULATIONS

The radii of curvature of the lenses in an optical system should be chosen so that spherical aberration and coma introduced by one element are minimized or cancelled by succeeding optical elements. This can be done by calculating the position factors of the elements involved (determined by image and object distances) and then choosing the best shape factor for each element which, in turn, fixes the radii of curvature of the lenses in the system.

Cancellation of spherical aberration is only possible for a combination of two or more lenses of opposite sign, viz., converging and diverging lenses. Coma, on the other hand, may be made positive, negative, or zero for a single lens by proper choice of shape factor (24). The parameters of our optical system were not sufficiently free to allow cancellation of spherical aberration; but the calculations for minimization of this effect were performed. Fortunately, the best shape factor for minimization of spherical aberration is very close to that for minimization of coma. After performing the necessary calculations, it was learned that converging cylindrical lenses other than plano-convex are excessively expensive. Plano-convex is, fortunately, close to the best lens

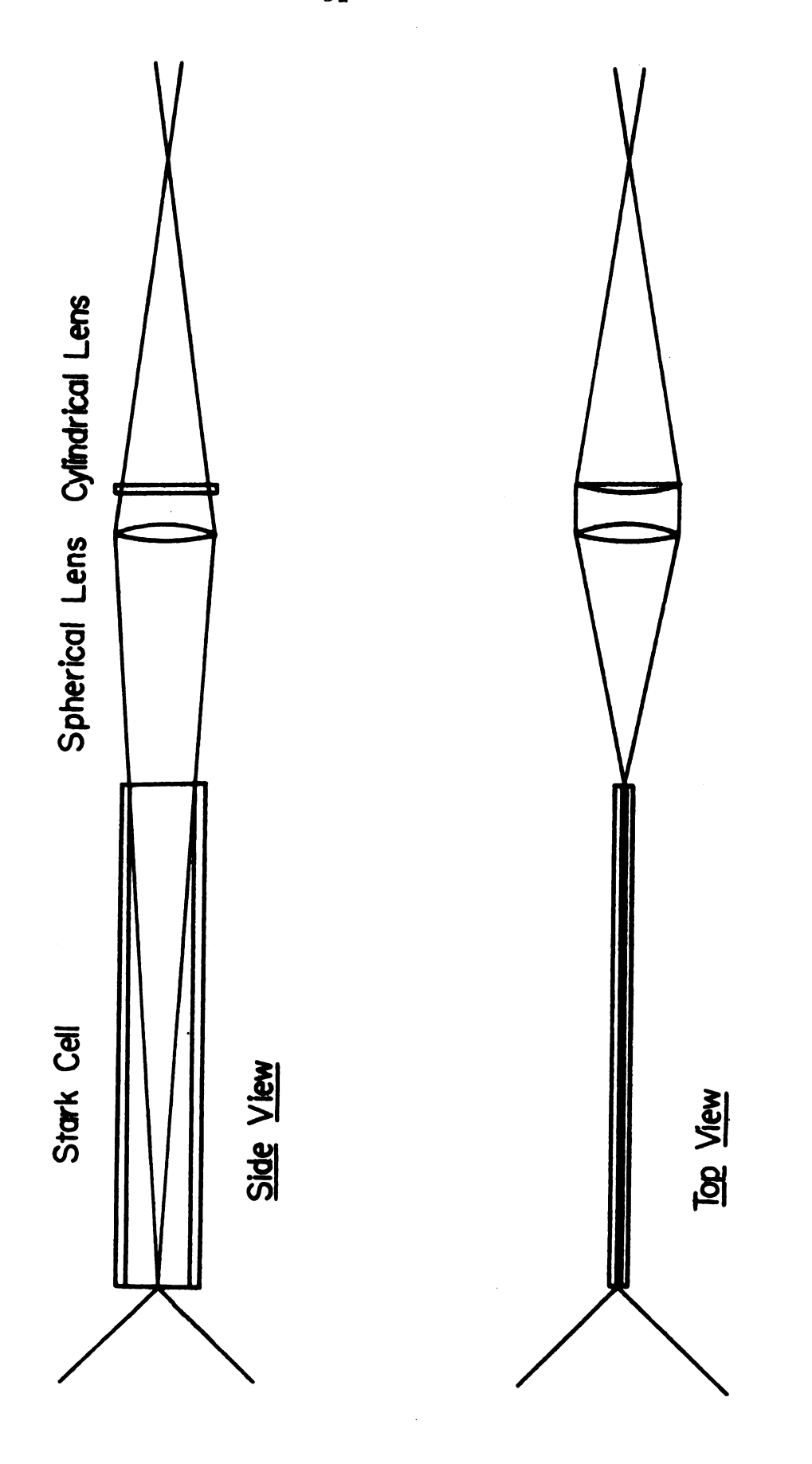


Figure (3.3) Fore-Optical System

shape for focusing collimated light. The following lens calculations are those for the cost-constrained lens system.

The horizontal (collimated) portion of the beam in the foreoptical system was measured to be approximately 6.5 cm. wide. Therefore, an f/10 converging cylindrical lens of focal length 65 cm. was
required. Since the index of refraction of  $CaF_2$  is approximately
1.42 in the near infrared and one radius of curvature  $r_2$  of this
lens was fixed by cost to be  $\infty$ , the other radius of curvature  $r_1$ is given by the lens makers' formula (24)

$$1/f = (n - 1)(\frac{1}{r_1} - \frac{1}{r_2}),$$
 (3.1)

to be 27.30 cm.

The spherical lens, on the other hand, has only its focal length (50 cm.) and the position factor p, given by (24)

$$p = \frac{s' - s}{s' + s} \tag{3.2}$$

fixed, where s' and s are the image and object distances, respectively. The position factor for this lens is of course different for the horizontal and vertical beams. The best shape factor q, to minimize spherical aberration, and hence the radii of curvature of this lens must be a compromise between the best values for the horizontal and vertical beams individually.

It is desirable that the horizontal portion of the beam be as free of spherical aberration and coma as possible because this part of the beam determines how many rulings on the grating of the monochromator are covered. The horizontal beam has object and image distances of s = 50 cm. and  $s' = \infty$ , respectively.

Therefore its position factor from (3.2) is p = +1.0. The best shape factor for reducing spherical aberration in a lens is given by (24):

$$q = \frac{-2(n^2 - 1)p}{n + 2}.$$
 (3.3)

For the horizontal beam, the best shape factor is q = -0.594. The vertical portion of the beam, on the other hand, has object and image distances of s = 150 cm. and s' = 75 cm., respectively. The vertical beam has a position factor of p = -1/3 and therefore a best shape factor of q = +0.198. The quantity  $L_s$ , which is a measure of the axial difference in focal length, is defined by (24):

$$L_{s} = \frac{1}{s'_{h}} - \frac{1}{s'_{p}}, \qquad (3.4)$$

or

$$L_{s} = \frac{h^{2}}{8f^{3}} \frac{1}{n(n-1)} \left[ \frac{n+2}{n-1} q^{2} + 4 (n+1)pq + (3n+2)(n-1)p^{2} + \frac{n^{3}}{n-1} \right],$$

where  $s'_h$  is the image distance for an oblique ray traversing the lens at a distance h from the axis and  $s'_p$  is the image distance of the paraxial ray. The quantity  $L_s$  was plotted for the horizontal and vertical beams as a function of the shape factor to find a compromise shape factor. q was chosen to be q = -0.50. The radii of curvature of the spherical lens are then given by (24)

$$r_1 = \frac{2f(n-1)}{q+1}$$
 and  $r_2 = \frac{2f(n-1)}{q-1}$ . (3.5)

With q = -0.50, f = 50.0 cm., and n = 1.42; the radii of curvature are  $r_1 = 84.0$  cm. and  $r_2 = -29.0$  cm. - the negative sign indicates surfaces curved in opposite directions. It is important that the

lenses face in the proper direction when in use. The two lenses were purchased from John Unertl Optical Co.

The two lenses were mounted on a large two axis cross slide that allowed accurate independent adjustments of each lens parallel and perpendicular to the light beam. The brass Stark cell housing was mounted on a specially designed three axis cross slide and connected to the fore-optical vacuum chamber (the shoe box) through an evacuated bellows. This arrangement allowed the walls of the fore-optical vacuum chamber to flex under atmospheric pressure without affecting alignment as well as providing easy external adjustments in focus and position.

## FREQUENCY CALIBRATION

Frequency measurements of EFS signals were made in the following manner. Absorption lines of an appropriate molecule or molecules whose frequencies bracket the frequency region of the EFS signal and whose frequencies are well enough known to be suitable as standards, are recorded before and after the EFS signal. The grating is never allowed to stop. Simultaneously, visible light Edser-Butler interference fringes having constant frequency spacing are recorded throughout the region of interest on the second pen of the dual pen recorder. The fringes provide a linear interpolation scale for frequency determination of the EFS lines lying between the standard frequencies. The details of this method are given by Olman (25) and by Rao, Humphreys, and Rank (26).

#### CHAPTER IV

## ELECTRIC FIELD INDUCED SPECTRA OF HCN

The linear molecule HCN was chosen as an experimental test of the new optical system because of its large permanent electric dipole moment (3 Debye), well spaced lines, and  $\ell$ -type doubling. The resulting induced spectra proved so interesting that a major part of the experimental effort was directed toward this molecule.

## Linear Molecules--General Features

The three normal vibrational modes of a linear tri-atomic molecule are shown in Figure (4.1). Two of these,  $\nu_1$  and  $\nu_3$  are non-degenerate while the bending mode,  $\nu_2$ , is two-fold degenerate, e.g., the molecule can bend in the plane of the paper or perpendicular to the plane of the paper.

The rotation-vibration absorption spectra of non-degenerate fundamental and overtone bands of linear molecules are extremely simple. Approximately evenly spaced R ( $\Delta J = +1$ ) and P ( $\Delta J = -1$ ) lines march out from the band origin where no Q ( $\Delta J = 0$ ) transitions are possible. In terms of axially symmetric molecules, the quantum number K, the projection of the total angular momentum along the molecular symmetry axis, is zero so that in an electric field only second order Stark effect is possible.

Transitions involving the two-fold degenerate  $\nu_2$  vibration are somewhat more complex both in the appearance of absorption bands and in the effects that an electric field may produce.

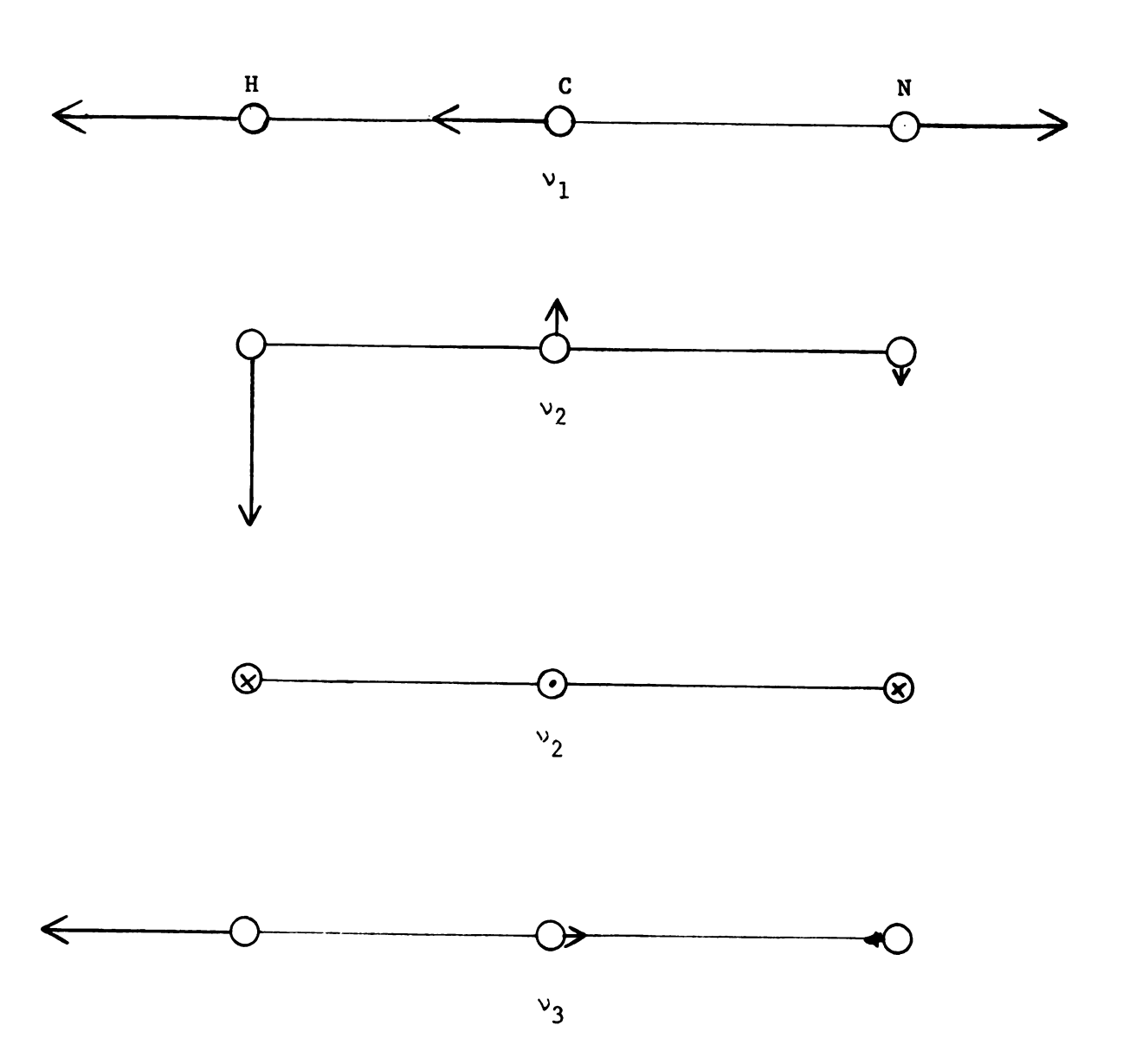


Figure (4.1) - Normal Vibrational Modes of HCN.

 $\nu_2$  has a fairly low frequency (712 cm<sup>-1</sup> for HCN) so that this state is appreciably populated at room temperature. Consequently, many fundamental and overtone rotation-vibration bands are accompanied by "hot bands", viz., transitions for which  $\nu_2$  is the lower vibrational state rather than the vibrational ground state.

The  $v_2$  vibration being essentially a two dimensional harmonic oscillator has an associated angular momentum. If  $v_2$  quanta of the  $v_2$  vibration are excited, a  $(v_2+1)$ -fold degeneracy is present and angular momenta (in units of  $h/2\pi$ ) of  $\ell=\pm \ell v_2-2$ ),  $\pm \ell v_2-4$ ),...,  $\pm 1$  or 0 are possible. If  $v_2=1$ , for example,  $\ell$  can be  $\pm 1$  corresponding to an angular momentum of rotation in either direction about the moelcular symmetry axis. Obviously, the total angular momentum quantum number must be greater than or equal to  $\ell$  in a degenerate vibration.

The  $(v_2+1)$ -fold degeneracy remains only to lowest order for the following reasons (16). A linear molecule excited to a degenerate vibrational state is formally analogous to a slightly asymmetric rotor. The angular momentum  $\ell$  is analogous to K in the limiting case symmetric top. Therefore in the symmetric top limit, states of the same magnitude of  $\ell$  are degenerate. Further small splittings of states having the same magnitude of  $\ell$  (commonly referred to as  $\ell$ -type doubling) takes place through the mutual interaction of the  $v_1$  and  $v_2$  vibrational states. The  $\Sigma^+$ ,  $v_1$  vibrational state lying above the  $v_2$  vibrational state (of symmetry  $\Pi$ ) in energy, interacts with the positive component  $\Pi^+$  of  $v_2$ . The negative component  $\Pi^-$  of  $v_2$  is unaffected. The interaction lowers the energy of the states belonging to  $\Pi^+$  with respect to those belonging to  $\Pi^-$  by an amount given by qJ(J+1), where q is approximately

constant within a given vibrational state (q = 0.007 cm<sup>-1</sup> for HCN (4) in the  $v_2$  fundamental).

For absorption spectra, the selection rules governing rotationvibration transitions of linear molecules are (16):

$$\Delta \ell = 0, \pm 1; \Delta J = 0, \pm 1 (J = 0 \neq J = 0); + \leftrightarrow -;$$

where the - (+) indicates whether the rotational wave function changes sign (doesn't change sign) under the inversion operation. Q branch transitions cannot occur when  $\mathcal{M} = 0$  and  $\ell = 0$ .

## The 3300 cm<sup>-1</sup> Region of HCN

When observed with zero field, the strongest absorption in the  $3300 \text{ cm}^{-1}$  region of HCN is due to the  $v_3$  fundamental, a  $\Sigma^+ - \Sigma^+$  transition. Accompanying this band at lower frequencies are the fairly strong "hot band"  $v_2 + v_3 - v_2$  ( $\Pi - \Pi$ ) and the  $2v_2 + v_3 - 2v_2$  ( $\Delta - \Delta$ ) "hot band" which is very weak at room temperature due to the Boltzmann factor. Another standard notation denoting these bands is  $(v_1, v_2^{\ell}, v_3)_{upper} - (v_1, v_2^{\ell}, v_3)_{lower}$ , e.g.,  $v_2 + v_3 - v_2$  is written  $(0, 1^1, 1) - (0, 1^1, 0)$ . In absorption, both bands are parallel bands ( $\Delta \ell = 0$ ) and have rotational selection rules  $\Delta J = 0, \pm 1$  so that R, P, and Q branches are allowed.

The calibration of this region was particularly simple because the frequencies of the  $v_3$  absorption lines are well known and commonly used as standards. The procedure during a calibrated EFS run was to admit a few Torr of HCN and run an absorption spectrum of the higher P(J) lines. The mechanical light chopper was then turned off and the absorption cell pressurized to  $\frac{1}{2}$  atm. with  $SF_6$ 

to prevent electrical breakdown while the grating continued to turn. The electric field was turned on and the EFS run. At the end of the EFS portion of the run, the electric field was turned off, the pressure of the HCN and  $SF_6$  mixture reduced to 2 cm., and the absorption spectrum of the higher R(J) lines run.

Figure (4.2) shows the observed electric field induced spectrum in this region. Positive signal represents an increase in absorption with the field on. Experimental conditions for this spectrum are given in Table (4.1).

## EFS of the $v_3$ Band of HCN

The  $\nu_3$  fundamental exhibits several interesting aspects of electric field induced spectra as well as allowing a "direct" measurement of the band origin.

The induced Q branch is clearly evident in Figure (4.2). The line shape is of type (a) as expected from the line shape expansion of Chapter II. Solely positive signal represents the difference between absorption with the field on and a lack of absorption without the field. The Q branch is made up of three partially resolved "lines". From formula (1.3), it is evident that the  $M=\pm 1\to M=0$  and  $M=0\to M=\pm 1$  transitions will be symmetrically displaced toward higher and lower frequencies, respectively, while the  $\Delta M=0$  transition is not displaced from the band origin. Table (4.2) shows calculated values of the relative intensities of the Q(0), Q(1), and Q(2) lines for electric field strengths near 30 Kv/cm. It is reasonable to assume from the values in the table, that only these three lines contribute significantly to the intensity of the observed induced Q branch. The splitting of the induced Q branch is

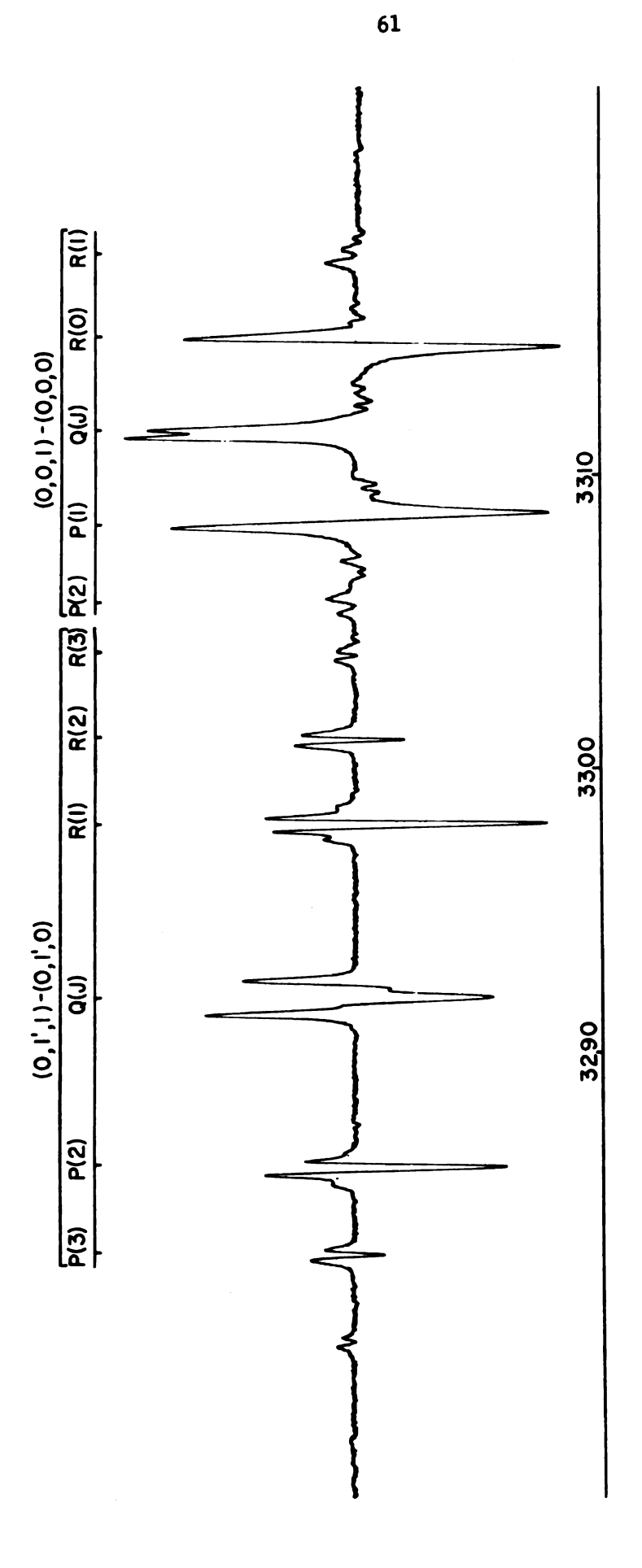


Figure (4.2) EFS of  $v_3$  and  $v_2 + v_3 - v_2$  Bands of HCN.

Molecule	ינ מ	Electric Bield	Sample	Spectrome		Cali-
	band	Fleid Strength (KJ/cm)	(Torr)	eter silt width (microns)	Detector	
HCN	v3 v2 <sup>t</sup> v3 <sup>-</sup> v2	61	-	70	Pbs Type P	
HCN	2 v <sub>3</sub>	19	17	077	Pbs Type O	
HCN	22+3-2		4	50	Pbs Type O	
DCN	v1tv3	19	Trace	70	Pbs Type O	

Table (4.1) Experimental Conditions for EFS of HCN and DCN.

attributable to partial resolution of the second order Stark effect components.

The apparent absence of observable  $\Delta M = 0$  transitions in the induced Q branch prompted polarization experiments because  $\Delta M = 0$  transitions occur for light polarized parallel to the field while  $\Delta M = \pm 1$  transitions occur for light polarized perpendicular to the field. It was found experimentally that in the 3 micron region our Stark cell transmitted about 8 times as much light energy polarized perpendicular to the field (in the plane of the cell height) as that polarized parallel to the field. Therefore, all of the spectra shown in this thesis are essentially recorded with light polarized perpendicular to the field direction.

Attempts to increase the resolution of the Q branch lines by decreasing the monochromator slit width were unsuccessful. The result of this operation was simply to decrease the intensity and eliminate some of the detail observed in the hot bands that are present. It was concluded that the pressure broadening due to the SF<sub>6</sub> was sufficient to make further resolution impossible.

Weak and noisy induced  $\Delta M=0$  transitions in the  $v_3$  Q branch of HCN were recorded by placing a silver chloride stacked plate polarizer in the light beam emergent from the Stark cell with the polarizer oriented to transmit light polarized parallel to the electric field.

The two side peaks of the EFS  $\,Q$  branch were measured at frequencies of 3311.335 cm<sup>-1</sup> and 3311.582 cm<sup>-1</sup>. The average frequencies of these two lines is 3311.458 cm<sup>-1</sup> and should be the frequency of the band origin. The low point between the two peaks was

Line Q(J)	Trensition  M  →  M'	Relative Intensity
Q (0)	0 → 0	0.09
	0 → 0	0.03
Q(1)	1 - 0	0.02
	1 - 1	0.02
	0 → 0	0.002
	1 - 0	0.001
Q(2)	1 - 1	0.001
	2 - 1	0.002
	2 -> 2	0.004

Table (4.2) Relative Intensities of Q Branch Transitions for HCN. (30 Kv/cm Electric Field)

measured to be 3311.465 cm $^{-1}$ . Both of these measurements agree within experimental error of approximately .015 cm $^{-1}$  with the calculated frequency of the band origin of 3311.4733 cm $^{-1}$  (27).

R(0) and P(1) in v<sub>3</sub> are striking examples of type (b)

EFS line shapes. All \( \Delta \mathbb{M} \) components of R(0) are shifted toward

higher frequency while all of those of P(1) are shifted toward

lower frequency by second order Stark effect (see equation (1.3)).

The difference between absorption with the field on and absorption

with the field off produces this characteristic up-down or down-up

asymmetric line shape. If all of the assumptions in the perturbation

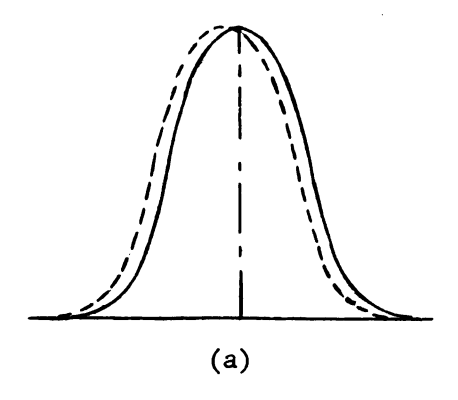
development of the line shape expansion were valid, an EFS type (b)

<sup>\*</sup> three standard deviations

line shape--first derivative of a Lorentzian line shape with respect to frequency--would have a zero at the central frequency of the absorption line in the absence of a field. The zero of the EFS P(1) line was measured at a frequency of 3308.467 cm<sup>-1</sup> compared to the value of Rank, et. al., (27), of 3308.5169 cm<sup>-1</sup>. The zero of R(0) was measured to be 3314.472 cm<sup>-1</sup> compared to the value of Rank, et. al., (27), of 3314.4089 cm<sup>-1</sup>. The larger discrepancy between these numbers is actually to be expected when the weak field assumption under which the line shape expansion was developed is examined for HCN.

The assumption that second order Stark splitting is too small for  $\Delta M$  type transitions to be resolved in HCN clearly doesn't hold because partial resolution was attained in the Q branch. The "smallness parameter",  $\mu F/JB$ , for the perturbation expansion of HCN is nearly unity for electric field strengths near 30 Kv/cm. With the electric field strengths used in this experiment, the theoretical model has been extended beyond its intended range, though the qualitative line shapes are in excellent agreement with the predictions of the model.

The measured zero of P(1) and the measured zero of R(0) should occur at lower and higher frequencies, respectively, than predicted by the expansion. The condition for the EFS line shape of P(1) to have a zero at the central frequency of the absorption line is shown graphically in Figure (4.3a). The induced line (shown dotted) has to have its position shifted toward lower frequency, its intensity increased, and perhaps have its envelope broadened by the field such that the induced line overlaps the absorption line (shown solid) precisely as shown in Figure (4.3a) for only then will the



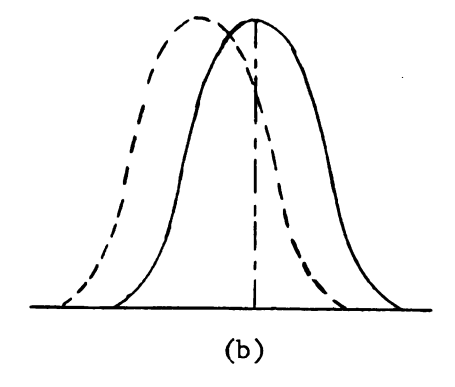


Figure (4.3) Overlapping in P(1) Transition in v<sub>3</sub> of HCN.

(Field = 0, indicated by solid line)

- (a) According to theory.
- (b) Experimentally observed.

difference between the intensities of these two lines be zero at the central frequency of the absorption line. Because of the large Stark shifts shown by HCN, P(1) would be expected to be shifted to a lower frequency than assumed in the expansion with the resulting zero of the EFS line shape also occurring at a lower frequency. This situation is shown in Figure (4.3b). The opposite effect would occur in R(0) and its EFS line shape zero would be expected at a higher frequency than theoretically predicted.

For higher values of the total angular momentum J, the P(J) and R(J) lines are asymmetrically broadened by the field, viz., not all of the  $\Delta M$  components for either type of line are shifted toward higher or lower frequency. In addition, the Stark splittings become smaller and the increase in intensity due to the field decreases rapidly with increasing J. Consequently, those few lines that are intense enough to be observable have asymmetric line shapes resembling EFS type (c) in the sense that positive-negative-positive signal is

observed. No quantitive conclusions have been derived from these weaker transitions.

EFS of the  $v_2 + v_3 - v_2$  Band of HCN

The electric field induced spectrum of the HCN  $v_2 + v_3 - v_2$  hot band exhibited several interesting effects arising from the  $\ell$ -type doubling of the upper and lower vibrational states.

Figure (4.4a) shows an energy level diagram of the upper and lower vibrational states for the  $v_2 + v_3 - v_2$  band including the (+) and (-) symmetry of the states with respect to inversion. The lowest member of each allowed transition is also indicated. (The  $\ell$ -type doubling of the J states has been exaggerated.)

In the presence of an electric field, the two nearly degenerate  $\pm \ell$  states for a given J value, having eigenfunctions  $\psi_1^o$  and  $\psi_2^o$  and unperturbed energies  $W_1^o$  and  $W_2^o$ , can interact strongly through the perturbation

$$-F\mu_{12} = -F \int \Psi_1^0 \mu \cos(\theta) \Psi_2^0 \sin(\theta) d\theta d\phi$$
 or 
$$-F\mu_{12} = -\frac{F \mu M}{J(J+1)} . \tag{4.1}$$

u is the average value of the electric dipole moment in the 2-type doubled state. The following results are taken from the lucid development of this problem given by Townes and Schawlow (4). Since a linear molecule excited to a degenerate vibrational state is formally equivalent to a slightly asymmetric rotor, the problem is also included in the general development of Stark effects in asymmetric rotors given by Golden and Wilson (28).

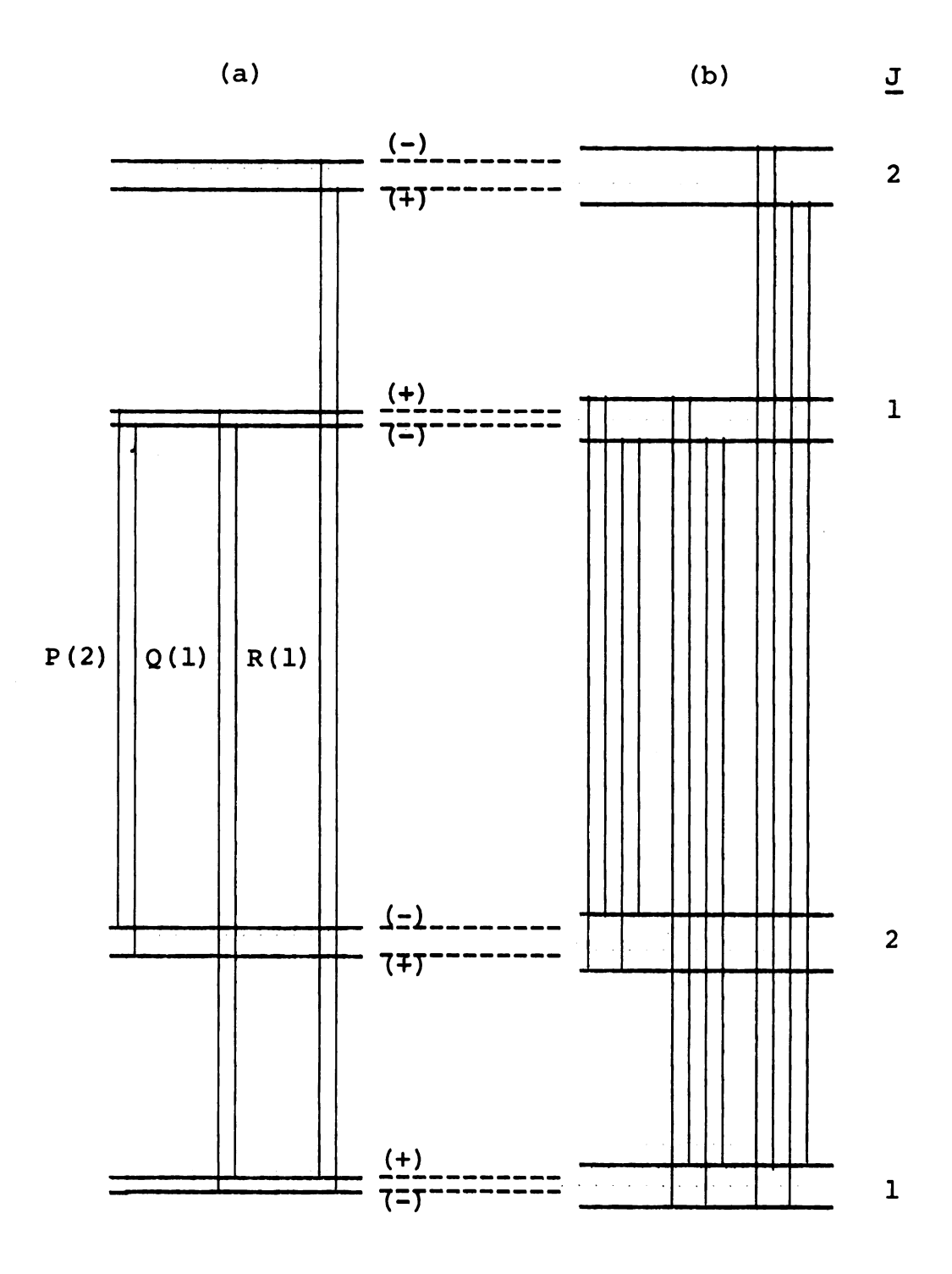


Figure (4.4) Transitions in  $\Pi$  -  $\Pi$  Band of Linear Molecules.

- (a) Electric Field = 0
- (b) Electric Field  $\neq 0$

The resulting energy shift obtained by solving the two dimensional secular equation for this degenerate perturbation theory problem is:

$$\Delta E = \frac{W_1^0 + W_2^0}{2} \pm \left( \left( \frac{W_1^0 - W_2^0}{2} \right)^2 + F^2 \mu_{12}^2 \right)^{\frac{1}{2}}, \tag{4.2}$$

where  $W_1^0 - W_2^0 = qJ(J+1)$  in this case.

The perturbed eigenfunctions are:

$$\psi_{1} = a(F)\psi_{1}^{\circ} + b(F)\psi_{2}^{\circ} 
\psi_{2} = -b(F)\psi_{1}^{\circ} + a(F)\psi_{2}^{\circ} ,$$
(4.3)

and

where the coefficients a(F) and b(F) are given by:

$$a(F) = \left\{ \frac{\sqrt{(W_{1}^{\circ} - W_{2}^{\circ})^{2} + 4F_{\mu_{12}}^{2} + (W_{1}^{\circ} - W_{2}^{\circ})}}{2\sqrt{(W_{1}^{\circ} - W_{2}^{\circ})^{2} + 4F_{\mu_{12}}^{2}}} \right\}^{\frac{1}{2}}$$

$$b(F) = \left\{ \frac{\sqrt{(W_{1}^{\circ} - W_{2}^{\circ})^{2} + 4F_{\mu_{12}}^{2} - (W_{1}^{\circ} - W_{2}^{\circ})}}{2\sqrt{(W_{1}^{\circ} - W_{2}^{\circ})^{2} + 4F_{\mu_{12}}^{2} - (W_{1}^{\circ} - W_{2}^{\circ})}} \right\}^{\frac{1}{2}}$$

$$(4.4)$$

If the degeneracy is nearly complete [as it is in HCN where  $(W_1^0 - W_2^0) = qJ(J+1)$  is small)], then (4.2) may be expanded

$$\Delta E = \frac{W_1^0 + W_2^0}{2} + F \mu_{12} . \qquad (4.5)$$

Thus, a "first order" Stark effect with a symmetric splitting of the degenerate  $\ell$  states occurs in the degenerate vibrational states of linear molecules.

If  $W_1^0 - W_2^0 = 0$ , (4.5) would be exact and be the magnitude of the result obtained by application of first order perturbation theory

to an axially symmetric rotor in the presence of a field. For a slightly asymmetric rotor, the two solutions of (4.5) describe the splitting of the nearly degenerate symmetric rotor limiting case states  $\pm$  K by the field.

Due to the mixing of the  $\pm \ell$  states through the field, both  $\ell$  components for a given J in the upper and lower vibrational states of a  $\Pi$  -  $\Pi$  transition contain (-) as well as (+) character and the (+  $\leftrightarrow$  -) selection rule allowing only two transitions between the two-fold degenerate upper and lower states breaks down. Consequently, <u>four</u> transitions are possible rather than the two allowed in the absence of the field. This is shown diagramatically in Figure (4.4b) for the lowest member of each type of allowed transition.

The R(1) EFS transition shown in Figure (4.2) is a splendid example of these field effects. The symmetric positive-negative-positive shape of the induced line is characteristic of EFS type (c) line shapes resulting from symmetric displacement of the two transitions allowed in the absence of a field. The weak, partially resolved positive signals flanking the main "line" are induced transitions corresponding to the field-free forbidden  $(+ \leftrightarrow +)$  and  $(- \leftrightarrow -)$  transitions having lower and higher frequencies than either of the field-displaced previously allowed  $(+ \leftrightarrow -)$  transitions. The ratio of the intensity of field-free forbidden  $(+ \leftrightarrow +)$  induced transitions to the intensity of the induced field-free allowed  $(+ \leftrightarrow -)$  transitions is shown below to be proportional to

$$\left[\frac{a'(F)b(F) - a(F)b'(F)}{a(F)a'(F) + b(F)b'(F)}\right]^{2}$$

a(F) and b(F) are the coefficients in the perturbed eigenfunctions

given in equations (4.3) and (4.4). Primes denote upper state coefficients. Thus, the comparitively weak induced transitions observed in the  $v_2 + v_3 - v_2$  band of HCN that are not allowed in the absence of a field are consistent with theoretical considerations because a'(F) and a(F) as well as b'(F) and b(F) will be nearly equal.

Figure (4.5) shows the upper and lower &-type doublet states participating in the transitions under consideration. The zero-field eigenfunctions and zero-field symmetry with respect to inversion are indicated for each of the four energy levels. A prime indicates the upper state. The example transition forbidden in the absence of a field is indicated by a broken line and the zero-field allowed transition is shown by a solid line.

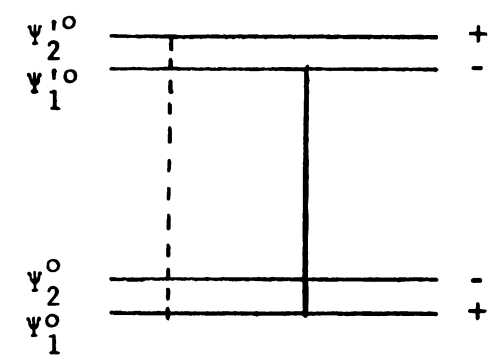


Figure (4.5) Energy Level Diagram of ¶ - ¶
Transitions in a Linear Molecule.

Solid line = allowed transition.

Broken line = forbidden transition.

The eigenfunction of the upper  $\ell$  level of the upper vibrational state in the presence of a field  $\Psi_{ii}^{l}$  is given by equation (4.3).

$$\Psi_{u}^{'} = -b'(F)\Psi_{1}^{'0} + a'(F)\Psi_{2}^{'0}.$$

As the field approaches zero, b'(F)  $\rightarrow 0$  and  $\Psi_u' \rightarrow \Psi_2'^0$  as it should. Similarly, the eigenfunction of the lower level of the lower

vibrational state in the presence of a field Y is given by

$$\Psi_{\ell} = a(F)\Psi_{1}^{\circ} + b(F)\Psi_{2}^{\circ}.$$

The transition moment between these two states is given by

$$\langle \Psi_{\ell} | \mu_{z} | \Psi_{u}^{'} \rangle =$$

$$\langle \{ a(F) \Psi_{1}^{O} + b(F) \Psi_{2}^{O} \} | \mu_{z} | \{ -b'(F) \Psi_{1}^{'O} + a'(F) \Psi_{2}^{'O} \} \rangle.$$

$$(4.6)$$

Only two of the four possible matrix elements on the right hand side of equation (4.6) are non-zero because of symmetry considerations.

Therefore, equation (4.6) reduces to

$$\langle \Psi_{\ell} | \mu_{z} | \Psi_{u}' \rangle = a'(F)b(F) \langle \Psi_{2}^{0} | \mu_{z} | \Psi_{2}^{10} \rangle$$

$$-a(F)b'(F) \langle \Psi_{1}^{0} | \mu_{z} | \Psi_{1}^{10} \rangle . \tag{4.7}$$

The two matrix elements in equation (4.7) are the changes in the dipole moment in going from the lower to the upper vibrational state and should be almost identical. Thus, the field induced transition moment for this transition is proportional to [a'(F)b(F) - a(F)b'(F)] and the intensity of the induced transition is proportional to  $[a'(F)b(F) - a(F)b'(F)]^2$ .

The eigenfunction of the lower  $\ell$  level of the upper state  $\Psi_{\ell}^{+}$  in the presence of a field is given by

$$\Psi_{\ell}^{\dagger} = a^{\dagger}(F)\Psi_{1}^{\dagger \circ} + b^{\dagger}(F)\Psi_{2}^{\circ \dagger}.$$

 $\Psi_{\ell}^{\dagger}$  reduces to  $\Psi_{1}^{\dagger O}$  as the field approaches zero because  $b^{\dagger}(F)$  goes to zero as  $F \to 0$ . Calculation of the transition moment for a transition between the lower state used in the preceding example and this upper state yields:

i

$$\langle \Psi_{\ell} | \mu_{z} | \Psi_{\ell}' \rangle = a(F)a'(F) \langle \Psi_{1}^{O} | \mu_{z} | \Psi_{1}^{O} \rangle$$

$$+ b(F)b'(F) \langle \Psi_{2}^{O} | \mu_{z} | \Psi_{2}^{O} \rangle.$$

Thus, the induced transition moment of this field-free allowed transition is proportional to [a(F)a'(F) + b(F)b'(F)] and the intensity of the induced transition is proportional to  $[a(F)a'(F) + b(F)b'(F)]^2$ . The ratio of the induced intensity of the field-free forbidden  $(+ \leftrightarrow +)$  transition to the induced intensity of the zero-field allowed  $(+ \leftrightarrow -)$  transition is therefore

$$\frac{\left[a'(F)b(F) - a(F)b'(F)\right]^2}{\left[a(F)a'(F) + b(F)b'(F)\right]^2}.$$

The absence of the R(0) and P(1) "missing lines" (because J cannot be zero in either state) is evident in the induced spectrum. Thus far, the author has found no satisfactory explanation for the line shape of the induced Q branch in the bands of HCN.

Listed in Table (4 1) are the measured frequencies of the stronger signals in the EFS of the  $v_3$  and  $v_2 + v_3 - v_2$  bands of HCN. The permanent electric dipole moment was calculated using the frequency splittings measured in the Q branch and equation (1.3) to be  $3.0 \pm 0.3$  Debye. Our value agrees within experimental error with the value measured by Maker of  $3.001 \pm 0.007$  Debye (5).

The spectacular electric field effects experimentally observed in the  $v_2 + v_3 - v_2$  hot band of HCN was the stimulus for further investigation of this molecule.

The 4000 cm<sup>-1</sup> Region of HCN

When observed with zero field, the strongest absorption in

Identification	Frequencies of Peaks	Polarity of Signal
Q(J) v <sub>3</sub>	3311.335	positive
	3311.582	positive
P(1) v <sub>3</sub>	3308.256	positive
	3308.661	negative
R(0) v <sub>3</sub>	3314.271	negative
	3314.668	positive
	3283.038	positive
$P(3) v_2 + v_3 - v_2$	3283.228	negative
	3283.307	positive
	3285.979	positive
$P(2) v_2 + v_3 - v_2$	3286.219	negative
	3286.459	positive
	3291.587	positive
$Q(J) v_2 + v_3 - v_2$	3292.129	neg <b>a</b> tive
	3292.734	positive
	3297.540	positive
	3297.830	positive
$R(1) v_2 + v_3 - v_2$	3298.058	negative
	3298.304	positive
	3298.668	negative
	3300.555	positive
$R(2) v_2 + v_3 - v_2$	3300.950	negative
	3301.140	positive

Table (4-1) EFS Frequencies in  $v_3$  and  $v_2 + v_3 - v_2$  of HCN.

the 4000 cm<sup>-1</sup> region of HCN is due to the perpendicular ( $\Delta \ell = 1$ )  $\Pi - \Sigma$  combination band  $\nu_2 + \nu_3$ . Accompanying this band are two perpendicular hot bands  $(0, 2^2, 1) - (0, 1^1, 0) \Delta - \Pi$  and  $(0, 2^0, 1) - (0, 1^1, 0) \Sigma^+ - \Pi$ . Only the upper state of  $\nu_2 + \nu_3$  is  $\ell$ -type doubled whereas both the upper and lower states of the accompanying hot bands exhibit  $\ell$ -type doubling. Unfortunately, frequency calibration in this region is much more difficult due to the lack of suitable wave-length standards and the band was not calibrated.

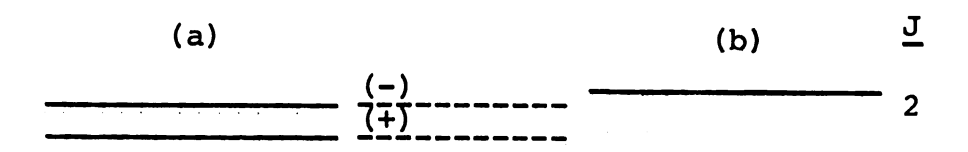
Figure (4.6a) shows an energy level diagram for the  $v_2 + v_3$  absorption band including the (+) and (-) symmetry with respect to inversion. The lowest member of each possible type of transition is also indicated. The  $\ell$ -type doubling of the various J states is greatly exaggerated.

In the presence of an electric field the nearly degenerate  $\pm \ell$  states for a given J value in the upper vibrational state interact producing the energy shifts and subsequent mixing of the (+) and (-) character of the states as described in the previous section. The resulting breakdown of the (+ +-) selection rule in the presence of a field makes each previously single transition a doublet as shown for the lowest member of the R, P, and Q branches in Figure (4.6b).

The interaction with the electric field lowers the energy of the lower  $\ell$ -type doubled level upon which all field free P and R branch lines terminate by an amount (in cm<sup>-1</sup>) given by:

$$\Delta E = -\mu_{12}F/hc, \qquad (4.8)$$

where the symbols are defined in the previous section. An allowed absorption line terminating on the lower &-type doubled level in the



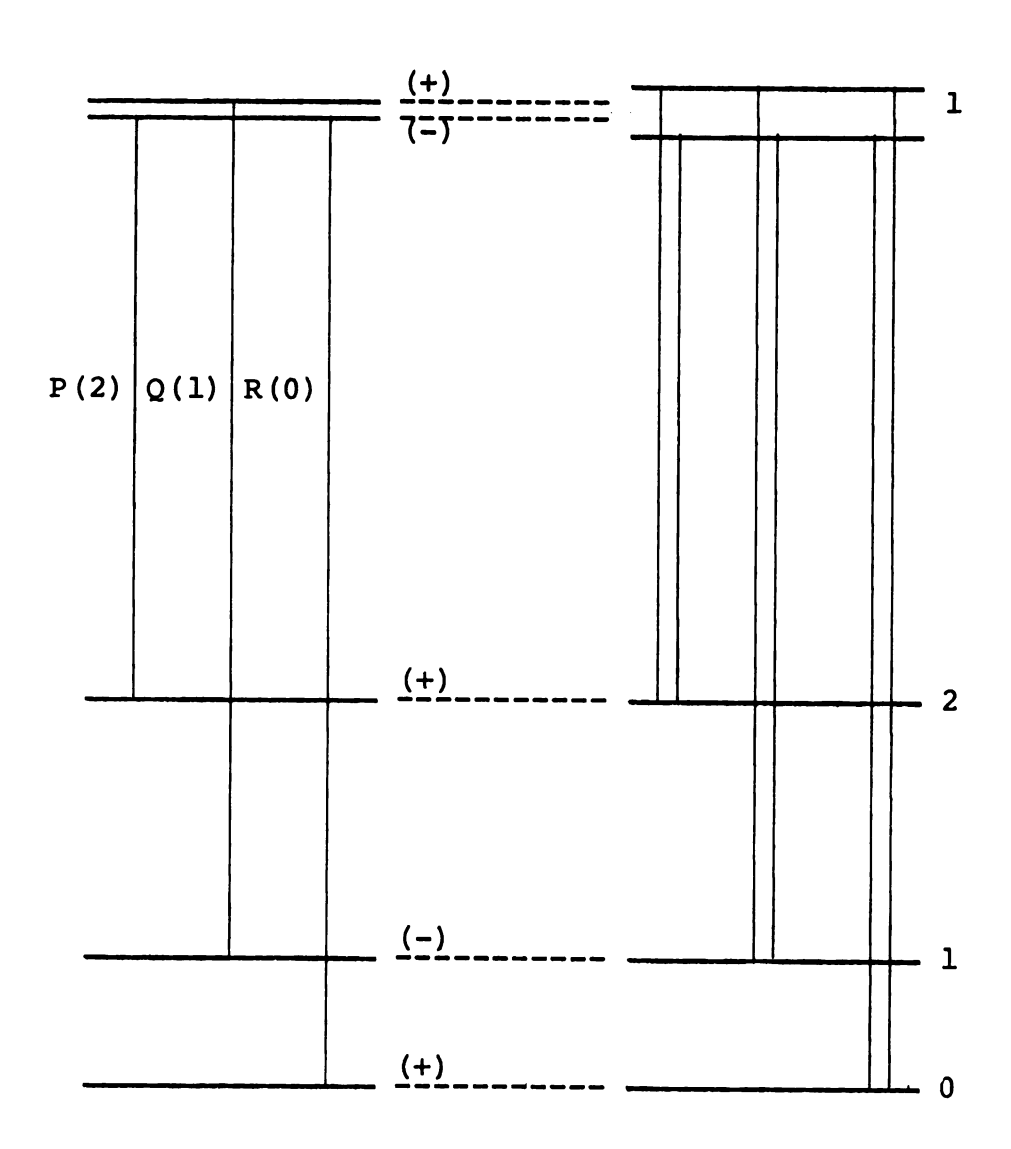


Figure (4.6) Transitions in  $\Pi - \Sigma$ Band of Linear Molecule.

- (a) Electric Field = 0
- (b) Electric Field  $\neq 0$

presence of the field will have its frequency lowered by the amount given in (4.8). The previously forbidden transition to the upper  $\ell$ -type doubled level will have a frequency higher than the allowed absorption transition by an amount determined by (4.8) plus qJ(J+1) due to Coriolis resonance described in the previous section.

A different induced intensity distribution would be expected for transitions in which only the upper (or lower) state exhibits  $\ell$ -type doubling. The perturbed eigenfunctions given by equation (4.3) may be applied to calculate the induced transition moments when only one state is  $\ell$ -type doubled. The following results are obtained from the calculation. The induced transition moment for the transition forbidden in the absence of a field is proportional to b'(F). The induced transition moment for the transition allowed in the absence of a field is proportional to a(F). The ratio of the intensities of these two induced transitions is therefore proportional to b'(F)/a(F), viz.,

$$[b'(F)/a(F)]^{2} \cong \frac{\sqrt{q^{2} + \frac{4\mu^{2}F^{2}M^{2}}{J^{4}(J+1)^{4}} - q}}{\sqrt{q^{2} + \frac{4\mu^{2}F^{2}M^{2}}{J^{4}(J+1)^{4}} + q}}.$$

With a field of 30 Kv/cm,  $\mu F \cong 0.8$  cm<sup>-1</sup> and  $q \cong 0.007$  cm<sup>-1</sup> for HCN. Thus, the induced zero-field forbidden transition in the  $v_2 + v_3$  band of HCN may be nearly as intense as the zero-field allowed transition.

Examination of the R branch line shapes in the spectrum shown in Figure (4.7) confirms the above analysis. In R(0) the two transitions allowed in the field are badly overlapped similar

to the situation shown in Figure (4.8). The R(J),  $J \neq 0$ , lines do not exhibit the overlapping to the same extent because the frequency separation between the zero-field absorption line and the induced transition terminating on the upper  $\ell$  level increases as qJ(J+1). The source of the small EFS signals on the high frequency side of R(5), R(6), etc., is not known. A weakly absorbing unidentified band in this region was observed in absorption surveys and these EFS lines may arise from that band.

Transitions in the P branch of  $v_2 + v_3$  should be of the same shape as those in the R branch but are overlapped by the lines of the  $(0, 2^2, 1) - (0, 1^1, 0)$  hot band. Note that P(1) is missing because the J = 0 level of the upper state cannot exist (J must be at least as large as  $\ell$ ).

For Q branch transitions the arguments given above concerning upper and lower  $\ell$  levels must be reversed because Q branch transitions all terminate on the upper  $\ell$  level in the absence of a field due to the  $(+ \leftrightarrow -)$  selection rule.

The  $v_2 + v_3$  Q branch which consists of solely positive signal in the spectrum in Figure (4.7) is a result of the high sample pressure. Figure (4.9) is a tracing of the line shape obtained for the Q branch with considerably lower pressure. Its shape is also EFS type (c), as expected. The asymmetry of the line is a result of the asymmetric shape of the absorption Q branch. The very strong unresolved Q branch in absorption spectra of perpendicular bands of linear molecules occurs only when there are nearly equal rotational constants B in the upper and lower vibrational states. The shape of the absorption Q branch is roughly triangular, trailing toward lower frequency. The strong positive

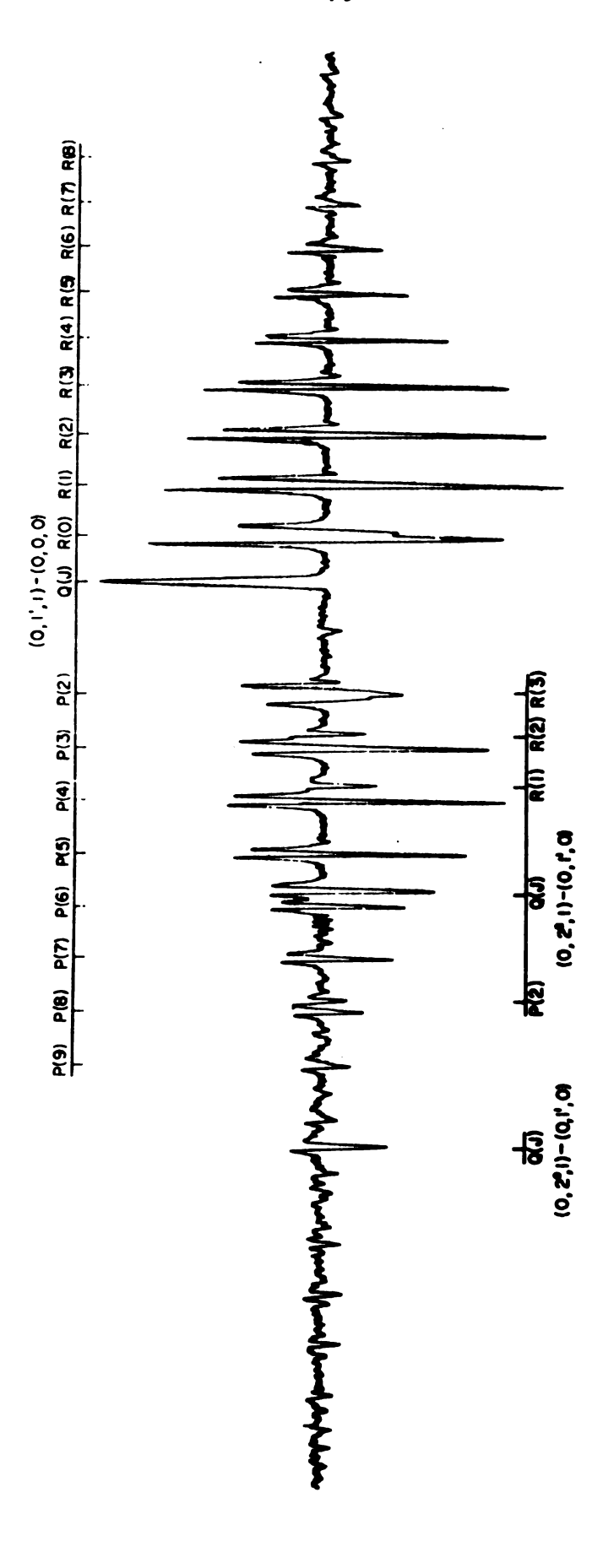


Figure (4.7) EPS of  $v_2 + v_3$  and  $2v_2 + v_3 - v_2$  Bands of HCH.

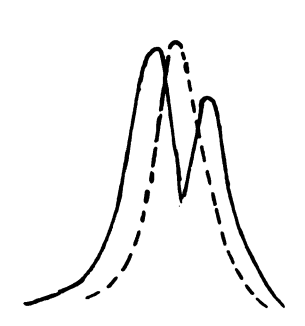


Figure (4.8) Overlapping in EFS R(0) Transition in  $\nu_2 + \nu_3$  Band of HCN. (Broken line is zero-field absorption)

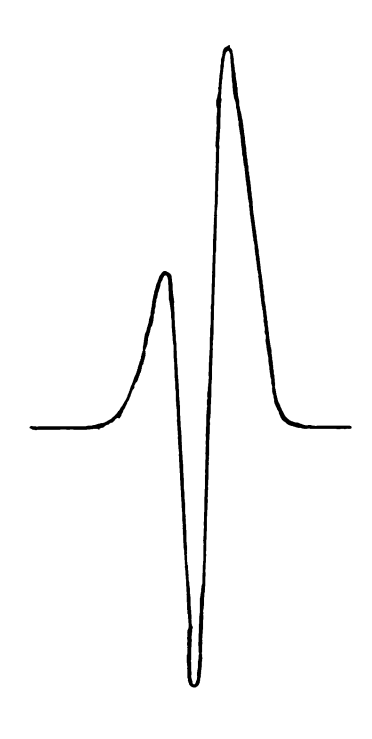


Figure (4.9) Tracing of Low Pressure HCN  $v_2 + v_3$  Band Induced Q Branch.

signal on the right hand side of the induced line is in the region where no zero-field absorption takes place. The weaker positive peak on the low frequency side is in the region where zero-field absorption takes place.

The two hot bands  $(0, 2^0, 1) - (0, 1^1, 0)$  at lower frequency and  $(0, 2^2, 1) - (0, 1^1, 0)$  shown in Figure (4.8) are essentially identical to the  $(0, 1^1, 1) - (0, 1^1, 0)$  hot band of the previous section except their line shapes are distorted by the overlapping P branch lines of  $v_2 + v_3$ .

# The 6500 cm<sup>-1</sup> Region of HCN

The  $2\nu_3$  band of HCN near 6500 cm $^{-1}$  is very similar to  $\nu_3$  in absorption as well as EFS and the EFS spectrum of this region was calibrated in the same manner as that of  $\nu_3$ , viz., using  $2\nu_3$  absorption lines as wavelength standards.

The induced Q branch at the band origin of  $2v_3$  was not as well resolved as that in  $v_3$ . The center of the Q branch "line" was measured to be 6519.597 cm<sup>-1</sup>. The frequency of the band origin of  $2v_3$  was calculated by Rank, et. al., (27), as 6519.6145 cm<sup>-1</sup>. The zeroes of the EFS line shapes of P(1) and R(0) were measured as 6516.603 cm<sup>-1</sup> and 6522.619 cm<sup>-1</sup>, respectively. The central frequencies of P(1) and R(0) are 6516.6581 cm<sup>-1</sup> and 6522.5286 cm<sup>-1</sup>, respectively.

The above results are consistent with those presented for  $v_3$  of HCN.

# The $v_1 + v_3$ Band of DCN

An electric field induced spectrum of the  $v_1 + v_3$  band of DCN near 4520 cm<sup>-1</sup> was run to compare with the results found in HCN. Unfortunately, so little of this gas was on hand that the resulting signals were extremely weak. The induced Q branch was barely discernable.

Frequency measurements of the induced lines in DCN were made in the same manner used for  $v_3$  and  $2v_3$  of HCN, viz., DCN absorption lines were used as wavelength standards.

The zeroes of the EFS P(1) and R(0) line shapes were measured at frequencies of 4520.774 cm<sup>-1</sup> and 4525.745 cm<sup>-1</sup>, respectively. The central frequencies of P(1) and R(0) measured by Rank, et. al., (29) are 4520.858 cm<sup>-1</sup> and 4525.656 cm<sup>-1</sup>, respectively.

The results for DCN are also consistent with those found in HCN.

The induced Q branch in DCN was too weak to measure.

#### CHAPTER V

# ELECTRIC FIELD INDUCED SPECTRA OF AXIALLY SYMMETRIC MOLECULES

Electric field induced spectra were observed for the following axially symmetric molecules:  $CH_3Br$ ,  $CH_3I$ ,  $CH_3Cl$ ,  $CH_3CN$ , and  $CH_3F$ . All attempts to obtain an induced  $CH_3D$  spectrum failed, probably because of its extremely small permanent electric dipole moment (0.01 Debye (30)). The induced spectra of the above molecules were very similar in appearance to one another and the spectrum of  $CH_3I$  is discussed as an example. The induced  $2v_5$  band of  $CH_3F$  is also discussed as an example of EFS parallel bands. Relative intensity measurements were made for selected transitions in the  $v_4$  induced spectrum of  $CH_3F$  in an attempt to determine the excited state dipole moment.

# The 3000 cm $^{-1}$ Region of $CH_3I$

Figures (5.1) and (5.2) show the electric field induced and absorption spectra, respectively, of the  $\nu_1$  and  $\nu_4$  bands of CH<sub>3</sub>I near 3000 cm<sup>-1</sup>. The electric field induced spectrum was obtained with a peak electric field strength of approximately 27 Kv/cm and sample pressure of 10 Torr. The Stark cell was pressurized to  $\frac{1}{2}$  atm. with SF<sub>6</sub> to prevent electrical breakdown. No frequency measurements were attempted for this molecule.

Absorption in the  $\nu_4$  band of CH  $_3$ I arises from changes in the electric dipole moment perpendicular to the molecular symmetry axis

and is consequently referred to as a perpendicular band. Selection rules governing changes in the K and J quantum numbers (the projection of the total angular momentum along the molecular symmetry axis and the total angular momentum, respectively) in perpendicular absorption bands are the following:

$$\Delta K = \pm 1$$
 and  $\Delta J = 0, \pm 1$ .

Spectroscopic notation denoting changes in J and K is similar to that for linear molecules, viz., P denotes a change of -1, Q corresponds to no change, and R denotes a change of +1. A particular transition is denoted by  ${}^{\Delta K}_{\Delta J_K}(J)$ , where  $\Delta K$  can be P or R for a perpendicular band and  $\Delta J$  can be P, Q, or R. In this notation, K and J refer to the lower state quantum numbers, e.g.,  ${}^PQ_1(2)$  denotes the transition from the state J=2, K=1 to the state J=2, K=0.

Absorption in the  $\nu_1$  band of CH $_3$ I arises from changes in the electric dipole moment parallel to the molecular symmetry axis and is consequently referred to as a parallel band. The selection rules obeyed by the rotational quantum numbers in a parallel band are  $\Delta K = 0$  and  $\Delta J = 0$ ,  $\pm 1$ .

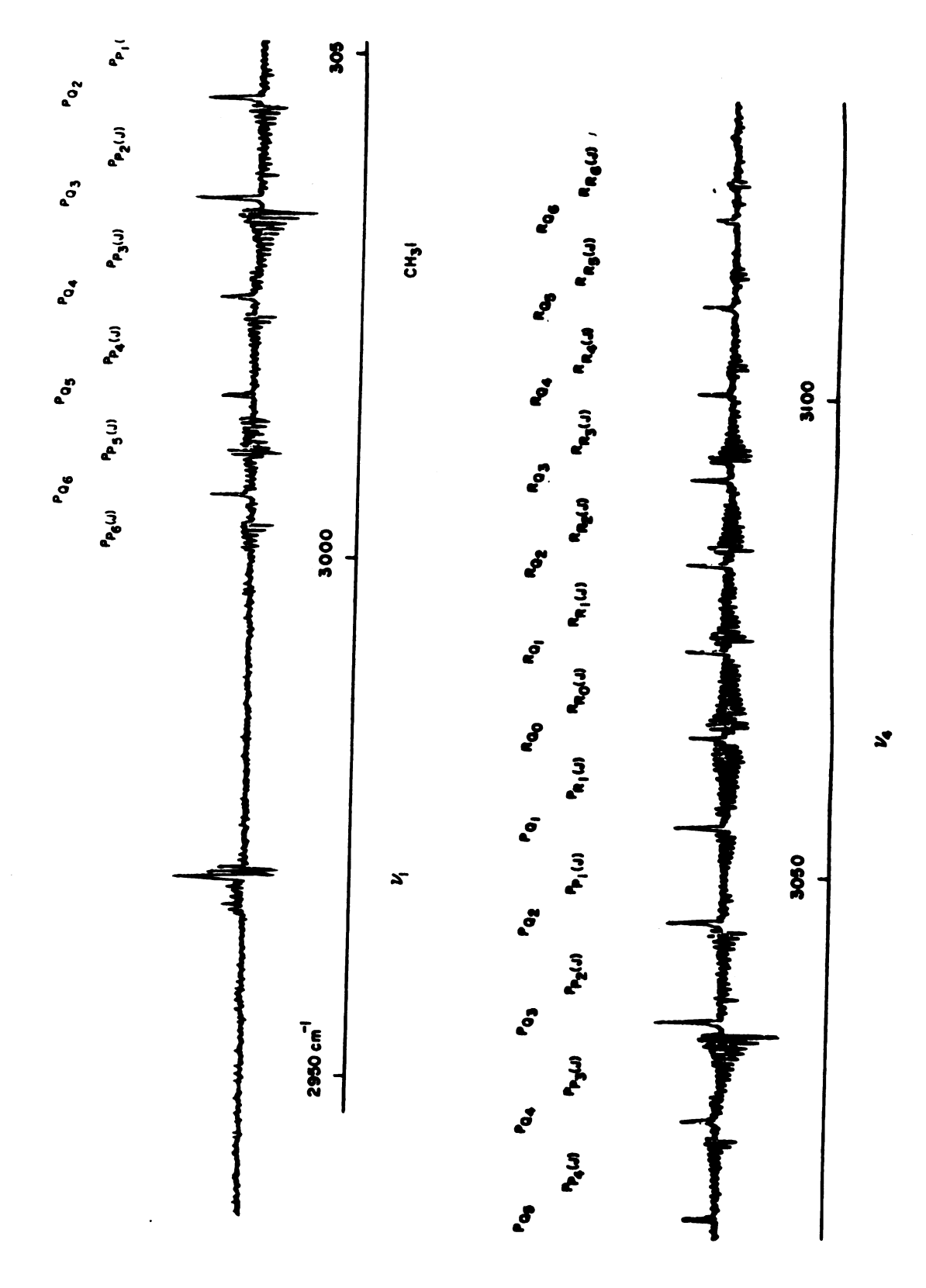
# Electric Field Induced Spectrum of the $v_4$ Band of $\text{CH}_3\text{I}$

Axially symmetric molecules exhibit first order Stark effect in all states where  $K \neq 0$  (c.f., equation (1.2)). EFS type (c) line shapes are therefore expected. The electric field symmetrically broadens the absorption line so that the difference between absorption with the field on and zero-field absorption has the characteristic EFS type (c) positive-negative-positive line shape. This is also the

case in transitions for which K=0 in perpendicular bands, viz.,  ${}^RR_0(J)$ ,  ${}^RP_0(J)$ , and  ${}^RQ_0(J)$  because although the lower state has K=0 so that no first order Stark effect is possible (c.f., equation (1.2)), the upper state has  $K\neq 0$  and a first order Stark effect is possible in this state. The K=0 case in the perpendicular band of a symmetric top molecule is similar to the EFS of the  $v_2+v_3$  band of HCN in which only one of the states involved in the transition exhibited first order Stark effect.

The induced  $\nu_4$  spectrum of  $\text{CH}_3\text{I}$  shown in Figure (5.1) beautifully illustrates EFS type (c) line shapes in the  $^R\text{R}_K(\text{J})$ ,  $^P\text{P}_K(\text{J})$ ,  $^P\text{P}_K(\text{J})$ ,  $^P\text{P}_K(\text{J})$ , and  $^R\text{P}_K(\text{J})$  series. Electric field induced enhancement of lower J transitions and attenuation of higher J transitions is apparent and consistent with intensity predictions (c.f., Table (2.7)). The influence of nuclear spin statistics is also apparent in the absorption spectrum, Figure (5.2), as well as in the induced spectrum. Those series in which K is zero or a multiple of 3 in the ground state have enhanced intensities as a result of the three-fold symmetry axis and the proton nuclear spin statistics.

The electric field induced spectrum of  $\nu_4$  demonstrates the usefulness of this experimental technique for making a large number of assignments of specific transitions in symmetric top spectra. Assignment of transitions in the typical symmetric top absorption spectrum is sometimes an arduous task of sorting out large numbers of closely lying lines. Comparison of the induced spectrum to the absorption spectrum shows that EFS clearly and uniquely picks out the low J transitions of a large number of series and makes their correct assignment almost trivial. This is one of the most useful



Pigure (5.1) EFS of v1 and v4 Bands of CH31.

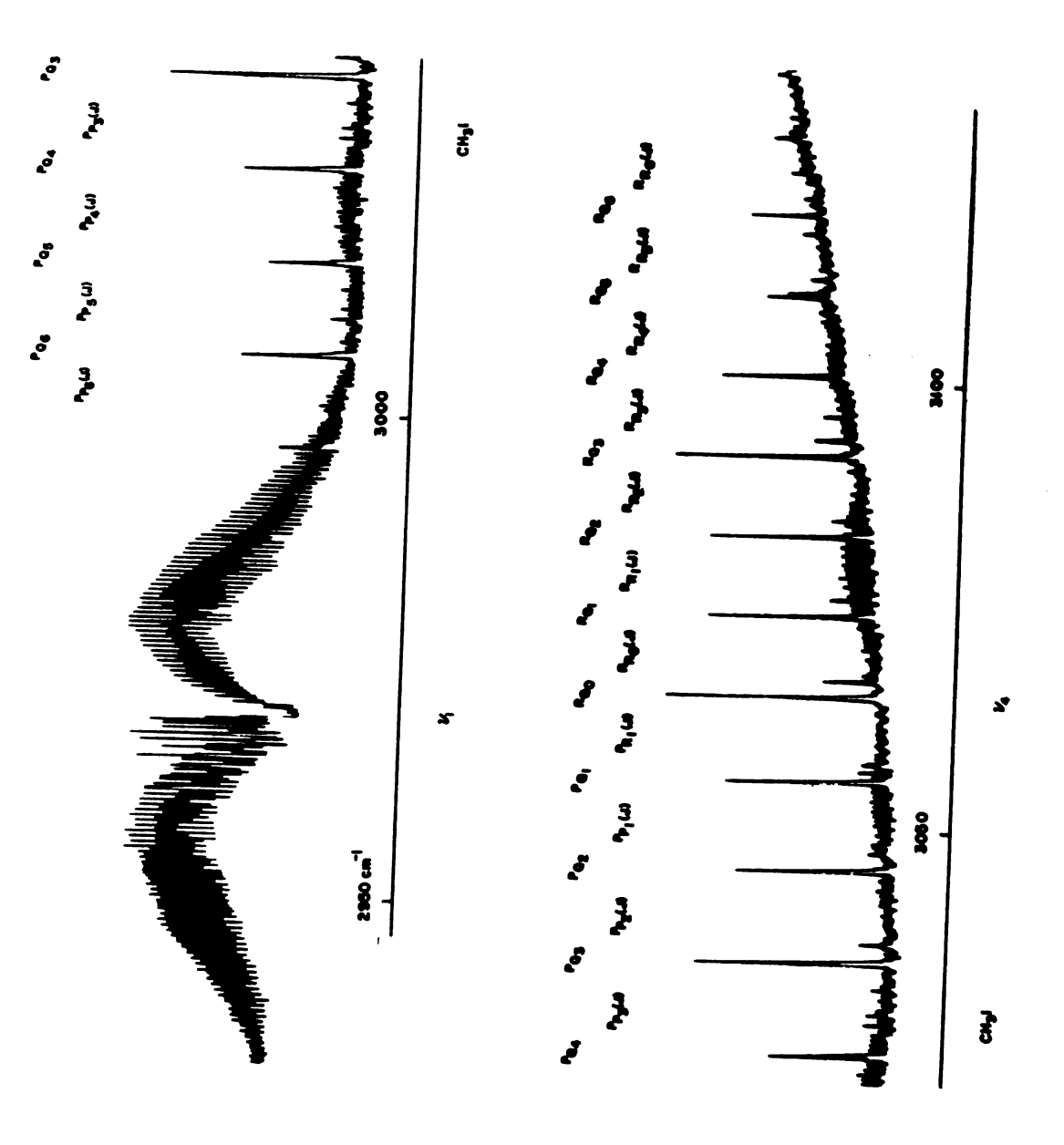


Figure (5.2) v1 and v4 Absorption Bands of CH31.

applications of this experimental technique for axially symmetric molecules.

Solely positive signal in the  $^RQ$  and  $^PQ$  branches is attributed to the high degree of overlapping of individual  $^RQ_K(J)$  and  $^PQ_K(J)$  transitions and high sample pressure. The induced  $^RQ$  and  $^PQ$  "lines" can be pictured as the difference between two "lines" one of which has a larger intensity due to the field than the other. These lines are analogous to the Q branch observed in the induced  $v_2 + v_3$  band of HCN. As was the case in HCN (c.f., Figure (4.9)), low pressure EFS of  $^RQ$  and  $^PQ$  branches in  $^PQ$  branches in  $^PQ$  exhibited asymmetrical EFS type (c) line shapes.

 $^{R}Q_{5}$  in CH $_{3}$ I is a "split" Q branch as shown in the absorption spectrum, Figure (5.2). In the induced spectrum, the right (high frequency) side of this split Q branch is much more intense than the left side. A possible interpretation of this line shape consistent with EFS intensity distributions is that the individual  $^{R}Q_{5}(J)$  transitions for lower values of J, say J=5 through J=10, are on the high frequency side and those of higher values of J are shifted toward lower frequency by the perturbation responsible for the splitting.

## Electric Field Induced Spectrum of the $v_1$ Band of $CH_3I$

Comparison of the  $\nu_1$  EFS in Figure (5.1) and the absorption spectrum in Figure (5.2) shows that only a few induced transitions near the band origin are present. This behavior is partly a result of high sample pressure. The  $\nu_1$  absorption band of a methyl halide is typically very strongly absorbing and overlaps the  $\nu_4$  fundamental to a considerable extent confounding assignments in both bands. With

the sample pressure required for the  $v_4$  EFS,  $v_1$  absorbs nearly 100 percent in the "wings" flanking the band origin. Consequently, changes in intensity in the "wing" regions are unnoticeable and no induced lines are observable. Those few lines appearing are near the band origin having low quantum numbers and occurring at frequencies where absorption is much less than in the wing regions.

A lower pressure EFS parallel band was obtained for CH<sub>3</sub>F.

Discussion of these transitions is deferred until those results are discussed.

## Electric Field Induced Spectra of $CH_3F$

Electric field induced spectra were observed and frequency measurements made for the following bands of  $CH_3F$ :  $\nu_1$ ,  $\nu_4$ ,  $2\nu_5$ ,  $\nu_1$  +  $\nu_3$  and  $\nu_3$  +  $\nu_4$ . The EFS line shapes observed in the  $2\nu_5$  band of  $CH_3F$  are described as examples of effects found in the parallel bands of axially symmetric molecules. A method of determining the ratio of the electric dipole moment in the upper vibrational state to that in the vibrational ground state through relative intensity measurements is presented and applied to the  $\nu_A$  vibration.

## Electric Field Induced Spectrum of the $2v_5$ Band of $CH_3F$

While EFS type (b) as well as EFS type (c) line shapes would be expected in parallel bands of an axially symmetric molecule, only EFS type (c) shapes were observed in these bands of CH<sub>3</sub>F.

The three types of absorption transitions in parallel bands, viz.,  ${}^QQ_K(J)$ ,  ${}^QP_K(J)$ , and  ${}^QR_K(J)$ , should exhibit EFS type (c) line shapes for  $K \neq 0$  because both states involved in the transition exhibit first order Stark effects. Several series of  ${}^QP_K(J)$  and

 $^{Q}R_{K}^{}$ (J) having EFS type (c) line shapes were observed in the  $^{2}v_{5}^{}$  band of  $^{CH}3^{F}$ . The identification of these series was again straightforward due to the weak EFS intensities of overlapping transitions involving higher quantum numbers.

The zero series transitions, viz., the  ${}^QQ_0(J)$  and the  ${}^QR_0(J)$ , should exhibit EFS type (b) line shapes. The reason for this expected behavior is that both states involved in the transition have K=0 and only second order Stark effect is possible.  ${}^QR_0(0)$  is completely analogous to R(0) in the  $v_3$  band of HCN.

It was not possible to identify any EFS type (b) line shapes in any of the parallel band EFS obtained. A possible explanation is the following. Based on the observed EFS of the  $\nu_3$  band of HCN, only the first line in either the  ${}^Q\!\!\!\!Q_0(J)$  or  ${}^Q\!\!\!\!R_0(J)$  series would be expected to be intense enough to be observable. Unfortunately, the region near the band origin of  $2\nu_5$  where these transitions should occur had an appearance resembling a damped sinusoidal oscillation. This appearance is possibly due to numerous Q branch transitions, but nothing distinct was identifiable.

## Electric Field Induced Spectrum of the $v_4$ Band of $CH_3F$

The method given below for determining the excited state electric dipole moment requires measurement of the relative intensities of selected transitions. It was found experimentally that EFS of the  $\nu_4$  perpendicular band of CH<sub>3</sub>F could be obtained at sample pressures so low that the  $^R$ R and  $^P$ P lines were not observable in the absorption spectrum of the CH<sub>3</sub>F-SF<sub>6</sub> mixture under the same experimental conditions. With this low a pressure, induced absorption will be very close to linear (exp [-kL]  $\cong$  k L). For this reason, the  $\nu_4$ 

band EFS of  $\text{CH}_3\text{F}$  was chosen for an experimental attempt to determine the ratio of the electric dipole moment in the  $v_4$  vibrational state to that in the vibrational ground state.

The intensity relationships for EFS type (c) lines in Table (2.7) are proportional to linear combinations of  $(K'\mu')^2$  and  $(K\mu)^2$ , where K' and K are the K quantum numbers of the upper and lower vibrational states, respectively.  $\mu'$  and  $\mu$  are the expectation values of the electric dipole moment in the upper and lower vibrational states, respectively. The intensity of an EFS type (c) transition from the state K=0 to K'=1 is, therefore, proportional to  $(\mu')^2$  and independent of  $\mu$ . Similarly, the intensity of an EFS type (c) transition from the state K=1 to the state K'=0 is proportional to  $(\mu)^2$  and independent of  $\mu'$ . The ratio of the intensity of a transition from K=0 to K'=1 to the intensity of a transition from K=0 should be proportional to  $(\mu'/\mu)^2$ .

Qualitative reasoning gives the same result. EFS type (c) line shapes arise from first order Stark effects and only states for which  $K \neq 0$  are affected by the field to first order. To first order therefore, only the upper state dipole moment of a K = 0 to K' = 1 transition interacts with the field, whereas, only the lower state dipole moment of a K = 1 to K' = 0 transition interacts with the field.

The following six series of lines in an axially symmetric molecule are suitable for use in such a determination of the upper state dipole moment:  ${}^{R}R_{0}(J)$ ,  ${}^{R}P_{0}(J)$ ,  ${}^{P}P_{1}(J)$ ,  ${}^{P}R_{1}(J)$ ,  ${}^{R}Q_{0}(J)$  and  ${}^{P}Q_{1}(J)$ . Individual lines in the last two series are not usually well enough resolved for the relative intensities of individual

transitions to be measured.

Substitution of K=0 or K=1 into the appropriate intensity formula in Table (2.7) yields the following relationships for the relative intensities of the four usable series of lines in  $CH_3F$ :

$$I \left( {}^{R}R_{0}(J) \right) = G \left[ \frac{4J+5}{(J+1)^{2}(2J+1)} \right] (\mu')^{2}$$

$$I \left( {}^{R}P_{0}(J) \right) = G \left[ \frac{4J-1}{J^{2}(2J+1)} \right] (\mu')^{2}$$

$$I \left( {}^{P}P_{1}(J) \right) = G \left[ \frac{4J+1}{J^{2}(2J+1)} \right] (\mu)^{2}$$

$$I \left( {}^{P}R_{1}(J) \right) = G \left[ \frac{4J+3}{(J+1)^{2}(2J+1)} \right] \mu^{2},$$
(5.1)

where G is a constant within a given band. The four ratios of equations (5.1) which will yield  $(\mu'/\mu)^2$  are the following:

$$I \begin{pmatrix} R_{R_0}(J) \end{pmatrix} / I \begin{pmatrix} P_{P_1}(J+1) \end{pmatrix} = \begin{bmatrix} \frac{2J+1}{2J+3} \end{bmatrix} (\mu'/\mu)^2$$

$$I \begin{pmatrix} R_{P_0}(J+1) \end{pmatrix} / I \begin{pmatrix} P_{R_1}(J) \end{pmatrix} = \begin{bmatrix} \frac{2J+3}{2J+1} \end{bmatrix} (\mu'/\mu)^2$$

$$I \begin{pmatrix} R_{R_0}(J) \end{pmatrix} / I \begin{pmatrix} P_{R_1}(J) \end{pmatrix} = \begin{bmatrix} \frac{4J+5}{4J+3} \end{bmatrix} (\mu'/\mu)^2$$

$$I \begin{pmatrix} R_{P_0}(J) \end{pmatrix} / I \begin{pmatrix} P_{P_1}(J) \end{pmatrix} = \begin{bmatrix} \frac{4J-1}{4J+1} \end{bmatrix} (\mu'/\mu)^2.$$

$$(5.2)$$

The statistical weights due to the effect of nuclear spin statistics have not been included in the above intensity ratios. The intensity of the K=0 lines in  $CH_3F$  must be divided by 2.

Two slow scan (0.01 degree/min. grating speed) EFS runs of the region of  $\nu_{\Lambda}$  containing those transitions suitable for use in the

dipole moment calculation were obtained. The following lines appeared to be free enough of influence from nearby lines to be usable:  ${}^RR_0(2)$ ,  ${}^RR_0(3)$ ,  ${}^RR_0(5)$ ,  ${}^RR_0(6)$ .  ${}^RR_0(9)$ ,  ${}^PP_1(2)$ ,  ${}^PP_1(3)$ ,  ${}^PP_1(6)$ , and  ${}^PP_1(9)$ . Using a triangular approximation, their areas were measured using a 6X magnifier for use as intensities in the calculations. All possible combinations of the above lines were used in formulas (5.1) to estimate the ratio of  $(\mu^*/\mu)$ . The fifteen sample values listed in Table (5.1) illustrate the results. The average value for the ratio of  $(\mu^*/\mu)$  was 0.9 with a maximum deviation of 0.5.

The electric dipole moment in the v<sub>3</sub> vibrational state of HCN has been measured using Stark effect frequencies to be only 0.5 percent larger than that in the ground vibrational state (5). The 0.5 percent change can be assumed to be a typical order of magnitude value for dipole moment changes due to molecular vibration. Even the most sophisticated present day methods of intensity measurement are incapable of high enough accuracy for determination of such small changes in electric dipole moments. If highly precise intensity measurements become possible in the future, this method of determining excited state electric dipole moments may prove more useful.

$\begin{array}{c} \text{J} \\ \text{of}  {}^{R}R_{0}^{}(\text{J}) \\ \text{Transition} \end{array}$	of ${}^{P}P_{1}(J)$ Transition	μ'/μ
2	2	0.7
2	3	1.0
2	6	0.8
2	7	1.2
3	2	0.6
3	6	1.4
3	7	1.0
5	2	0.6
5	3	0.6
5	6	1.0
5	7	1.7
6	3	0.5
6	6	0.9
6	7	1.0
9	7	0.8

Table 5.1 Measured Ratio of  $\nu_4^{}$  and Ground State Electric Dipole Moments for  ${\tt CH}_3{\tt F}.$ 

#### CHAPTER VI

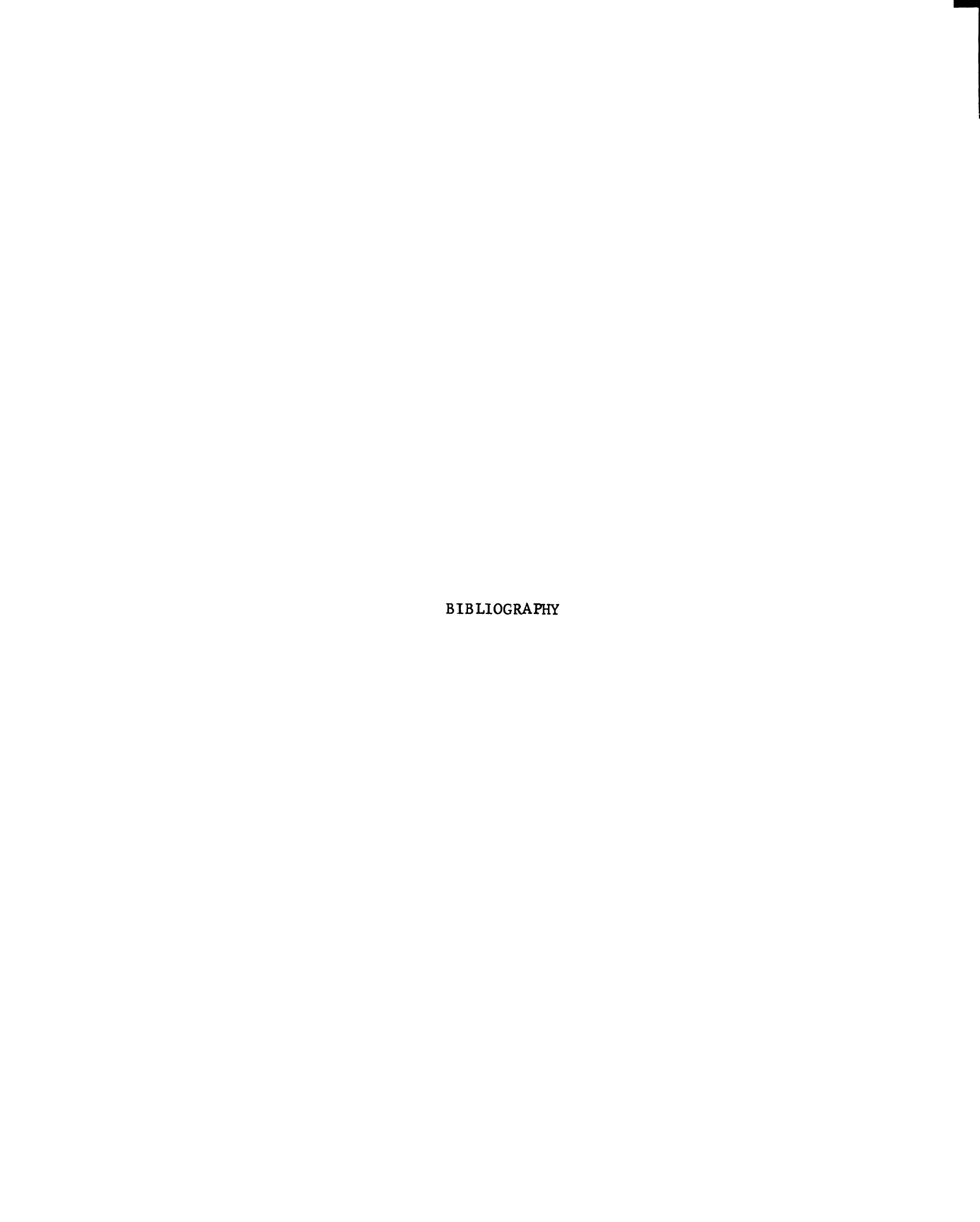
#### CONCLUSIONS

EFS appears to be a useful new tool for infrared spectroscopists. Observed EFS exhibit line shapes and intensities in good qualitative agreement with theoretical predictions. In the linear molecule HCN, for example, we observed line shapes corresponding to two different types of normally forbidden transitions, second order Stark effect, first order Stark effect, and intensity enhancement due to  $\ell$ -type doubling. For all of the axially symmetric molecules, we found EFS a valuable tool in assigning transitions because those transitions involving states of low angular momenta are very much stronger than those involving states of higher angular momenta. From the ratios of intensities of EFS transitions in the  $\nu_4$  band of  $\text{CH}_3\text{F}$ , we obtained an estimate of the excited state electric dipole moment. Improved experimental techniques should eventually lead to more quantitative results.

### Suggestions for Future Development

Several improvements should be made in the present electric field induced spectrum apparatus. First, a Princeton Applied Research (PAR) phase sensitive lock-in amplifier (or better) in conjunction with a precision reference frequency doubler should provide a substantial increase in information to noise ratio and allow operation at an optimum detection frequency. This piece of apparatus would also be of benefit to those interested primarily in absorption

spectra. Secondly, a dc amplifier to enable simultaneous recording of absorption and EFS signals would provide a useful frequency calibration method as well as greatly facilitating transition identifications. Thirdly, the optimum dimensions and separation of a Stark cell for use in EFS studies should be experimentally determined. Finally, if the spectral deconvolution studies about to be undertaken in our laboratory prove successful and experimental improvements can be made in the EFS apparatus to obtain an order of magnitude better resolution, useful information about line widths and excited state electric dipole moments could be obtained from induced spectra.



#### **BIBLIOGRAPHY**

- 1. E.U. Condon, Phys. Rev. 41, 759 (1932).
- 2. M.F. Crawford and R.E. MacDonald, Can. J. Phys. 36, 1022 (1958).
- 3. R. Terhune and C. Peters, J. Mol. Spectry. 3, 138 (1959).
- 4. C.H. Townes and A.L. Schawlow, "Microwave Spectroscopy". McGraw-Hill, New York, 1955.
- 5. P.D. Maker, thesis, University of Michigan, 1961.
- 6. J.H. Shirley, J. Chem. Phys. 38, 2896 (1963).
- 7. A.D. Buckingham, Proc. Roy. Soc. A. 267, 271 (1962).
- 8. A.D. Buckingham and D.A. Dows, Disc. Faraday Soc. 35, 48 (1963).
- 9. D.A. Dows and A.D. Buckingham, J. Mol. Spectry. 12, 189 (1964).
- 10. H. Eyring and G. Kimball, 'Quantum Chemistry', John Wiley and Sons, Inc., New York, 1944.
- 11. G. Placzek and E. Teller, Z. Physik 81, 209 (1933).
- 12. M.W.P. Strandberg, "Microwave Spectroscopy". John Wiley and Sons, Inc., New York, 1954.
- 13. N.J. Bridge, D.A. Haner, and D.A. Dows, J. Chem. Phys. <u>48</u>, 4196 (1968).
- 14. R.S. Knox and A. Gold, "Symmetry in the Solid State". W.A. Benjamin, Inc., New York, 1964.
- 15. G.W. King, "Spectroscopy and Molecular Structure". Holt, Rinehart, and Winston, Inc., New York, 1964.
- 16. G. Herzberg, "Molecular Spectra and Molecular Structure". Van Nostrand, Princeton, New Jersey, 1945.
- 17. G. Amat, Compt. rend. 250, 1439 (1960).
- 18. A. Sayvetz, J. Chem. Phys. 7, 383 (1939).

- 19. S.S. Penner, 'Quantitative Molecular Spectroscopy and Gas Emissivities'. Addison-Wesley, Reading, Massachusetts, 1959.
- 20. H.G. Heard, "Laser Parameter Measurements Handbook". John Wiley and Sons, New York, 1968.
- 21. Donald B. Keck, thesis, Michigan State University, 1967.
- 22. Joseph A. Aubel, thesis, Michigan State University, 1964.
- 23. C.W. Peters, Personal communication.
- 24. F.A. Jenkins and H.E. White, "Fundamentals of Optics". Third Edition, McGraw-Hill Book Company, New York, 1957.
- 25. Melvin D. Olman, thesis, Michigan State University, 1967.
- 26. K.N. Rao, C.J. Humphreys, and D.H. Rank, 'Wavelength Standards in the Infrared'. Academic Press, New York, 1966.
- 27. D.H. Rank, G. Skorinko, D.P. Eastman, and T.A. Wiggins, J. Mol. Spectry. 4, 518 (1960).
- 28. S. Golden and E.B. Wilson, Jr., J. Chem. Phys. 16, 669 (1948).
- 29. D.H. Rank, G. Skorinko, D.P. Eastman, and T.A. Wiggins, J. Opt. Soc. Am. 50, 421 (1960).
- J.S. Muenter, M. Kaufman, and W. Klemperer, J. Chem. Phys. 48, 3338 (1968).

MICHIGAN STATE UNIVERSITY LIBRARIES
3 1293 03143 2556